

SW-HIR-168

HIRDLS

High Resolution Dynamics Limb Sounder

ALGORITHM THEORETICAL BASIS DOCUMENT

ATBD-HIR-01

Calibration and Geo-location of HIRDLS radiances

4th October 1999

See <http://www.atm.ox.ac.uk/user/wells/atbd.html> for latest version

Any comments on this document may be addressed to wells@atm.ox.ac.uk

CHANGE HISTORY

15-Jan-1999 Original Version. Submitted to ATBD Review Panel chaired by Larry Gordley (GSFC 18-May-1999).

06-Jul-1999 Corrected typos. Changed "boresight" to "principal optical axis". Used "chopper period" instead of "chopper frequency". Removed references to accelerometers. Removed e_{BB} from expression for calibrated radiance in Section 3.8. Incorporated changes to Level 1 file description agreed at L1 Science Software Review meeting (Oxford 01-Jul-1999).

12-Jul-1999 Changed latitude, longitude and time items in Level 1 file contents description to "standard" HDF-EOS names and types. Added rad_flag description.

13-Jul-1999 Added Spacecraft velocity (ECI mm/s) to Level 1 file contents

27-Aug-1999 Revised Level 1 file contents description to use HDF structure names and to add View Direction item. Added draft Appendix 5.2.

10-Sep-1999 Revised some HDF structure names and modified Appendix 5.2.

23-Sep-1999 Edits to 5.2.1 and change cold filter temperature from LNS2TMP to FPA_TEMP

4-Oct-1999 Added Recommendation 3 response to Appendix 5.2. Submitted to PSO as requested in e-mail from Jim Closs dated 23 July 1999.

CONTENTS

1. [Introduction](#)

- 1.1 Purpose and [Scope](#)

2. [Overview and Background Information](#)

- 2.1 HIRDLS [Experiment Description](#)
- 2.2 Data [Processing Environment](#)
- 2.3 Algorithm [Heritage](#)
- 2.4 [Lessons Learned](#) from ISAMS

3. [Calibration Algorithms](#)

- 3.1 [Raw Data Quality Control](#)
- 3.2 [Engineering Telemetry Conversion](#)
- 3.3 [Spacecraft Location](#)
- 3.4 [Spacecraft Attitude](#)
- 3.5 [Instrument Pointing](#)
- 3.6 [Tangent Point Location](#)
- 3.7 [Celestial Bodies in Field of View](#)
- 3.8 [Radiometric Calibration](#)
- 3.9 [Error Estimation](#)

4. [Processing Considerations](#)

- 4.1 [Data Volumes](#)
- 4.2 [Numerical Computation Considerations](#)
- 4.3 [Data Flow](#)
- 4.4 [File Formats](#)
- 4.5 [Quality Control and Diagnostics](#)
- 4.6 [Exception Handling](#)
- 4.7 [Coding Standards](#)

5. [Appendices](#)

- 5.1 [Applicable Documents](#)
- 5.2 [CHEM-1/SOLSTICE ATBD Review, May 18-19, 1999.](#)

- 5.3 [Acronyms and Abbreviations](#)
-

1. INTRODUCTION

1.1 PURPOSE and SCOPE

The requirement for this document is a CDRL (No 601) for HIRDLS specified in *GSFC 424-28-21-03* and due for review 48 months before launch. In a letter from Michael King to PIs dated 6 May, 1998 delivery to EOS Project Science Office on 15 Jan 1999 was requested.

The purpose of this document is to describe the algorithmic basis for the software to be used to convert HIRDLS Level 0 data (raw counts of the spacecraft telemetry) to Level 1 data. In Level 1 data, radiances and engineering data are calibrated and expressed in conventional units. In addition, information about the location of observations is derived from ephemerides and instrument pointing data. This document is restricted to the discussion of algorithms used in the production of standard HIRDLS products and does not address the use of research and calibration data obtained in special observation modes (e.g. spacecraft pitch-down, moon-viewing).

2. OVERVIEW and BACKGROUND INFORMATION

HIRDLS is an experiment to be flown on the EOS-CHEM satellite as a part of the NASA EOS program and is collaborative effort between Oxford University in the UK (PI J.J. Barnett) and the University of Colorado in Boulder, USA (PI J.C. Gille). The science goals of HIRDLS are to observe the global distributions of temperature and several trace species in the stratosphere and upper troposphere at high vertical and horizontal resolution.

Further details can be found in [Gille, J. C. and J. J. Barnett: Conceptual Design of the High Resolution Dynamics Limb Sounder \(HIRDLS\) for the EOS Chemistry Mission.](#)

The instrument will obtain profiles over the entire globe, including the poles, both day and night. Complete Earth coverage (including polar night) can be obtained in 12 hours. High horizontal resolution is obtained with a commandable azimuth scan which, in conjunction with a rapid elevation scan, typically provides a 2,000 to 3,000 km-wide swath of profiles along the satellite track. Vertical profiles are spaced every 4 degrees in latitude and 5 degrees in longitude, with 1 to 1.5 km vertical resolution.

2.1 HIRDLS EXPERIMENT DESCRIPTION

HIRDLS is an infrared limb-scanning radiometer designed to sound the upper troposphere, stratosphere, and mesosphere to determine temperature; the concentrations of O₃, H₂O, CH₄, N₂O, NO₂, HNO₃, N₂O₅, ClONO₂, CFC11, CFC12, and aerosols; and the locations of polar stratospheric clouds and cloud tops. The goals are to provide sounding observations with

horizontal and vertical resolution superior to that previously obtained; to observe the lower stratosphere with improved sensitivity and accuracy; and to improve understanding of atmospheric processes through data analysis, diagnostics, and use of two- and three-dimensional models.

The optical system with a telescope consisting of a plane scan mirror, a parabolic primary and ellipsoidal secondary mirror, is shown schematically in Figure 1.

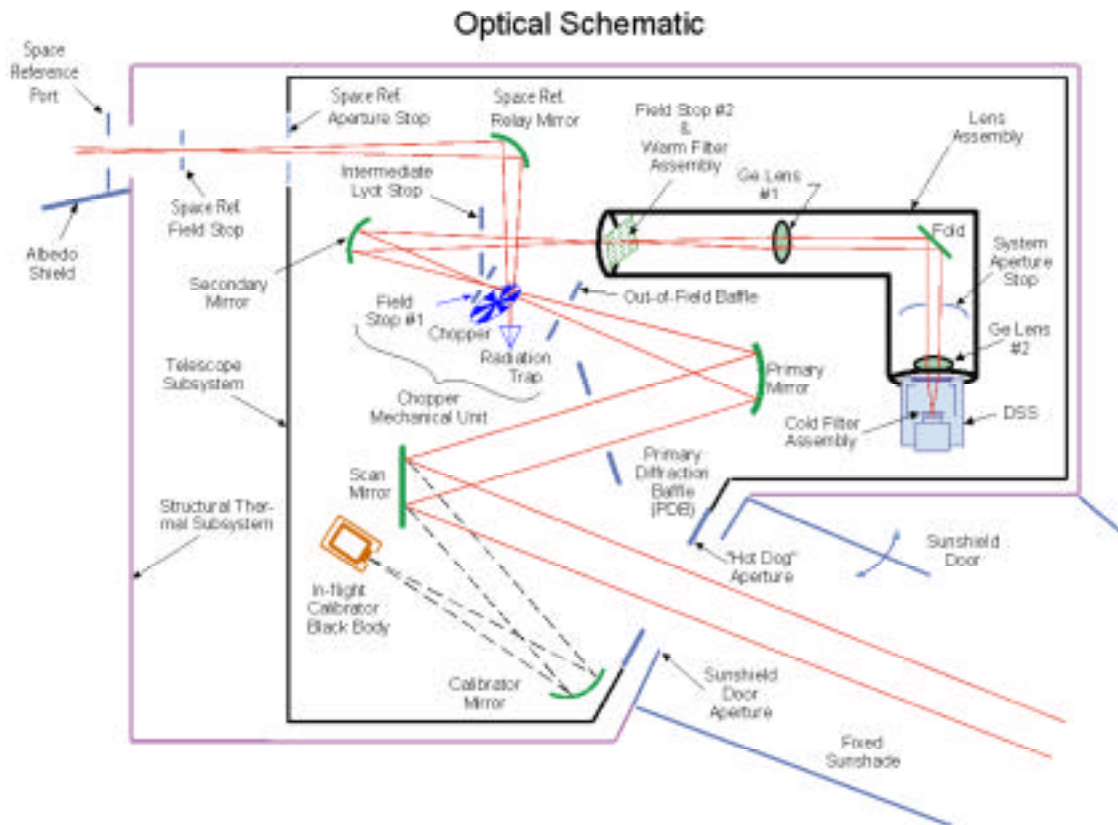


Figure 1.

Other components critical to the radiometric calibration discussed in this document are the chopper, the space reference relay mirror and the in-flight calibrator mirror. The scan mirror rotates about both azimuth and elevation axes. High-precision pointing information is obtained by the use of gyroscopes mounted on the instrument optical bench to measure changes in alignment in space of the primary optical axis.

The chopper wheel has six gaps and rotates at a nominal commandable frequency of 83.3Hz. This produces a nominal 500Hz cycle in the detector signal waveform. In normal operation, all HIRDLS telemetry timing is based on the sync pulse generated once per revolution by the chopper. The primary telemetry sample rate is once per chopper revolution (c. 12ms). A science data packet is generated every eight chopper revolutions (a minor frame) i.e. c. 96ms. A major frame consists of 8 minor frames, 64 chopper revolutions, and lasts approximately 768ms. All telemetry points (listed in [section 3.2](#)) are sampled at least once during a major frame. This is also the interval allowed for all the SAIL tasks (mentioned later and described in [SAIL Software Requirement Document SW-HIR-147A](#)) to complete an operation cycle.

HIRDLS performs limb scans in the vertical at multiple azimuth angles, measuring infrared emissions in 21 channels ranging from 6.12 to 17.76 micron. Each channel uses two separate band pass interference filters and a photoconductive HgCdTe detector cooled by Stirling cycle device. Details of the detector layout can be seen in the field of view map, Figure 2.

Field-of-View Map

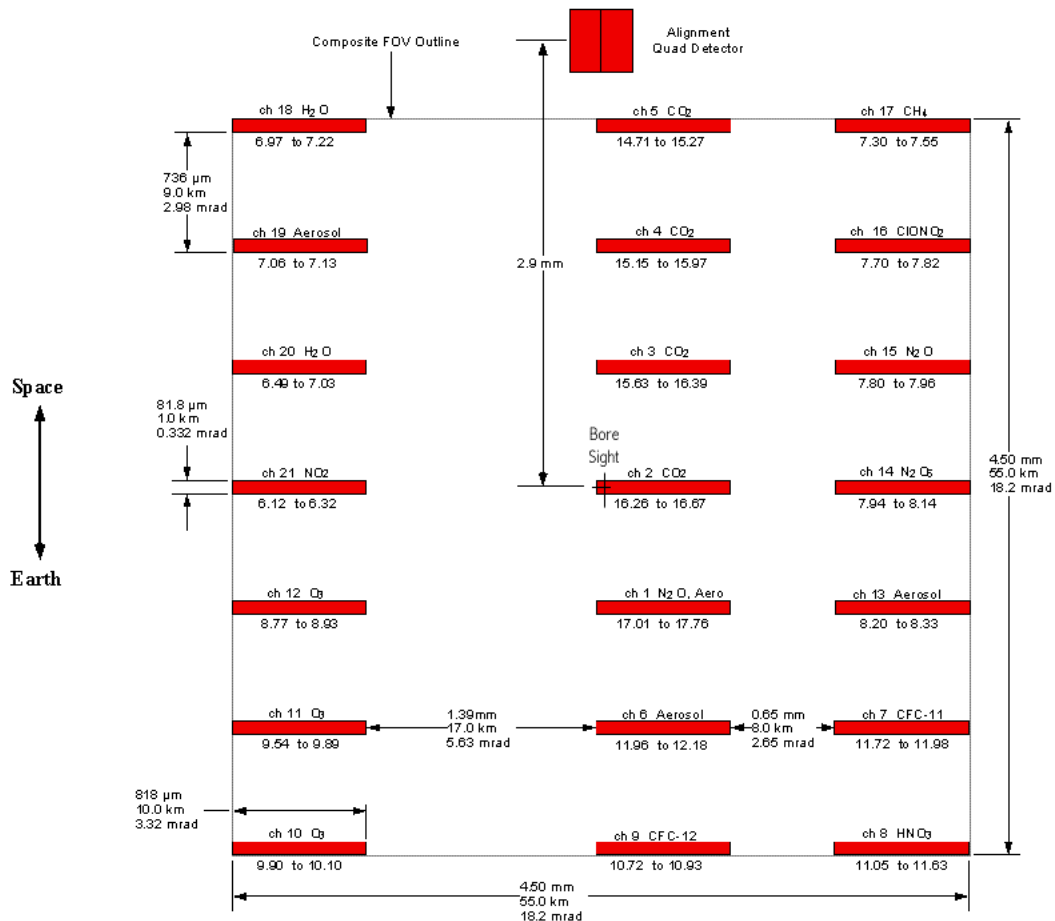


Figure 2.

Four channels measure the emission by CO₂. Taking advantage of the known mixing ratio of CO₂, the transmittance is calculated, and the equation of radiative transfer is inverted to determine the vertical distribution of the Planck black body function, from which the temperature is derived as a function of pressure. Once the temperature profile has been established, it is used to determine the Planck function profile for the trace gas channels. The measured radiance and the Planck function profile are then used to determine the transmittance of each trace species and its mixing ratio distribution.

Winds and potential vorticity are determined from spatial variations of the height of geopotential surfaces. These are determined at upper levels by integrating the temperature profiles vertically from a known reference base. HIRDLS will improve knowledge of data-sparse regions by measuring the height variations of the reference surface provided by conventional sources with the aid of a gyro package. This level (near the base of the stratosphere) can also be integrated downward using nadir temperature soundings to improve tropospheric analyses.

HIRDLS raw instrument data rate is approximately 60 kbps.

The instrument is controlled in routine operations by Science Algorithm Implementation Language (SAIL) programs running in the Instrument Processor Unit (IPU). These programs generate observation sequences which are used to control the scan mirror and instrument pointing. In addition the programs also monitor instrument health and safety and control such things as the operation of the sunshield door. However these functions are not within the scope of this document.

The Scan Pattern shown below will be used as the basis for the design of the Scanner control hardware and software. It is representative of all scan patterns in the azimuth direction. In the elevation direction it is representative of an operational scan profile with respect to peak-to-peak amplitude and average offset. The ultimate operational offset may be larger or smaller, depending on the ephemerides achieved after launch. A more comprehensive set of profiles, and the way in which they have been derived, will be found in SP-HIR-198.

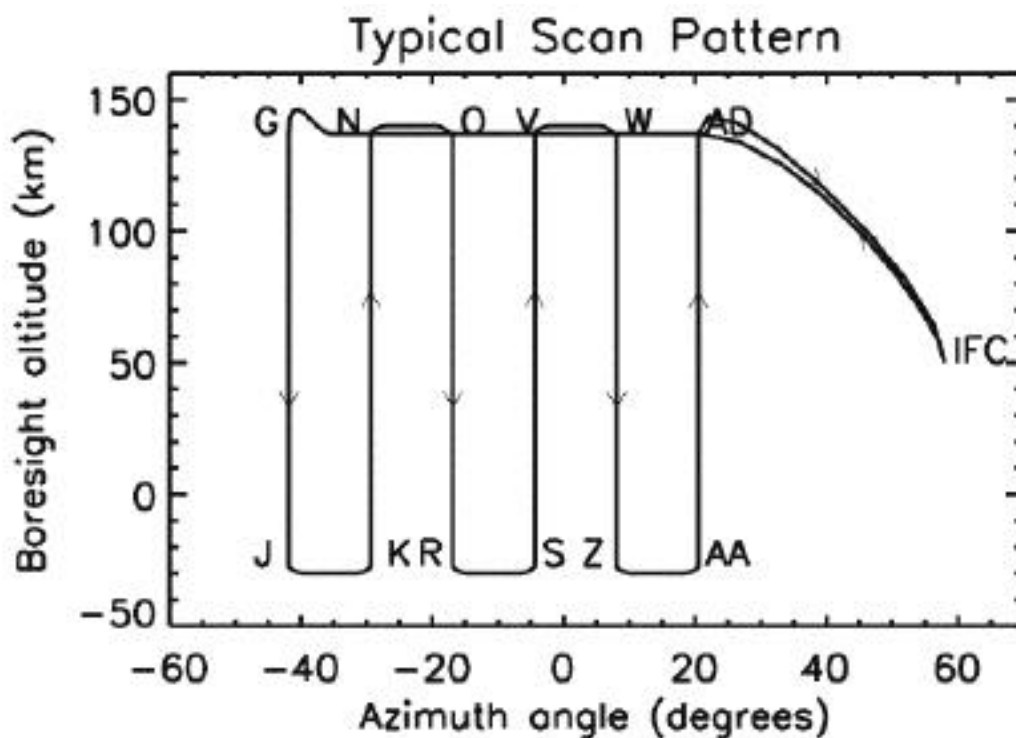


Figure 3.

Figure 3 shows scan mirror elevation angles (expressed in terms of boresight altitudes) plotted against azimuth angles in a full scan sequence which takes approximately 65 seconds to complete. The coordinates for points on the sequence A, B, C ... AE are given in the following table.

	Elevation shaft angle (deg)			Azimuth shaft angle (deg)	Time (s)	Tangent point height (km)	
	Low	Nominal	High				
A	TBD	TBD	TBD	TBD	0.00	N/A	Start at IFC view
B	-1.64	-1.11	-0.53	10.25	1.87	137.0	Azimuth scan at space
C	-1.62	-1.10	-0.52	4.02	2.16	137.0	view elevation
D	-1.61	-1.09	-0.52	-2.21	2.44	137.0	
E	-1.63	-1.11	-0.53	-8.44	2.79	137.0	
F	-1.67	-1.13	-0.54	-14.67	3.23	137.0	
G	-1.72	-1.17	-0.56	-20.90	4.31	137.0	Elevation scan 1 (down)

H	-1.37	-0.83	-0.23	-20.90	5.31	105.4	
I	-1.34	-0.80	-0.20	-20.90	5.41	103.0	
J	0.03	0.53	1.09	-20.90	13.15	-27.0	
K	0.03	0.51	1.05	-14.67	14.15	-27.0	Elevation scan 2 (up)
L	-1.30	-0.77	-0.20	-14.67	21.89	103.0	
M	-1.32	-0.80	-0.22	-14.67	21.99	105.4	
N	-1.67	-1.13	-0.54	-14.67	23.00	137.0	
O	-1.63	-1.11	-0.53	-8.44	23.99	137.0	Elevation scan 3 (down)
P	-1.29	-0.78	-0.21	-8.44	24.99	105.4	
Q	-1.27	-0.76	-0.19	-8.44	25.09	103.0	
R	0.03	0.50	1.03	-8.44	32.83	-27.0	
S	0.03	0.50	1.01	-2.21	33.83	-27.0	Elevation scan 4 (up)
T	-1.25	-0.75	-0.19	-2.21	41.57	103.0	
U	-1.28	-0.77	-0.21	-2.21	41.67	105.4	
V	-1.61	-1.09	-0.52	-2.21	42.67	137.0	
W	-1.62	-1.10	-0.52	4.02	43.67	137.0	Elevation scan 5 (down)
X	-1.28	-0.77	-0.21	4.02	44.67	105.4	
Y	-1.26	-0.75	-0.19	4.02	44.77	103.0	
Z	0.03	0.50	1.02	4.02	52.51	-27.0	
AA	0.03	0.50	1.03	10.25	53.51	-27.0	Elevation scan 6 (up)
AB	-1.27	-0.76	-0.19	10.25	61.24	103.0	
AC	-1.30	-0.78	-0.22	10.25	61.34	105.4	
AD	-1.64	-1.11	-0.53	10.25	62.34	137.0	
AE	TBD	TBD	TBD	TBD	64.78	N/A	Dwell at IFC view
A	TBD	TBD	TBD	TBD	65.28	N/A	

Notes:

1. This table is based on the sequences shown in tables 4, 5 and 6 of SP-HIR-198, with the timing taken from table 5.
2. The sections of each elevation scan between -27 and +103 km and between +105.4 and +137 km should be scanned at constant elevation shaft angle rates. The short section between 103 and 105 km is provided to enable the rate to change.
3. The tangent point height is given for the boresight.
4. The elevation and azimuth shaft angles for the IFC view are intentionally not specified here.
5. Line-of-sight angles are approximately double the shaft angles.
6. This table is intended as an example of how the scanner may be required to operate in the baseline mode. It is for example possible that the sequence may be required in the reverse order, or that a greater number of separate constant rate segments may be required within each elevation scan.

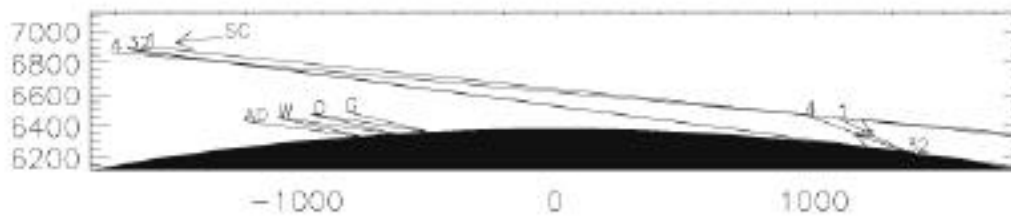


Figure 4.

Figure 4 (which assumes a spherical earth and circular satellite orbit and ignores the effects of azimuth scanning) shows the main features of the changes in (Channel 5) tangent point location. Axes are labelled in kilometers. HIRDLS views to the rear of the spacecraft. As the instrument looks higher in the atmosphere so the tangent point approaches the spacecraft. The lowest tangent points (2 and 3) are approximately 3080km from the spacecraft, the highest tangent points (1 and 4) are approximately 2715km from the spacecraft, a difference of 365km. During a single 'vertical' scan (1 to 2, or 3 to 4) the spacecraft moves approximately 65km so the horizontal span of a profile is approximately 300km for a down scan or 430km for an up scan. The span of the full scan profile of Figure 3 is also illustrated.

2.2 DATA PROCESSING ENVIRONMENT

Algorithms for processing HIRDLS instrument data are developed by the PI team and delivered to NASA as Science Data Product (SDP) Software for installation in an EOSDIS data processing facility. The SDP software resulting from this document will be designed, coded and tested on the Oxford University Science Computing Facility (SCF). The software will then be transferred to the HIRDLS team at UCB who are responsible for the integration of all HIRDLS production processing software into EOSDIS.

2.3 ALGORITHM HERITAGE

The HIRDLS instrument has a very long heritage from several instruments flown on the NIMBUS and Upper Atmosphere Research Satellite (UARS) spacecraft. The most recent and relevant experience was with the Improved Stratospheric and Mesospheric Sounder (ISAMS) instrument on UARS which involved most of the main features of HIRDLS except for the instrument gyroscopes. Algorithms for processing ISAMS data were coded and delivered to NASA for use in routine product generation in a very similar way to that planned for the EOS programme. The approach used for in-flight radiometric calibration and a discussion of the results was published by

C.D. Rodgers et al in the Journal of Geophysical Research, 101, 9775-9794, 1996.

2.4 LESSONS LEARNED FROM ISAMS

The main problem that the ISAMS algorithms needed to address was the large orbital change in thermal environment of a satellite radiometer (typically two spacecraft terminator crossing per orbit). Almost all the engineering telemetry showed a large orbital signature even in cases where

components were tightly thermostated. As these signatures tended to be in phase it was very difficult to determine the partial derivatives (dependencies) precisely. For example, a telemetry point could vary with supply voltage and temperature but the voltage and temperature could themselves exhibit very similar variations. Most dependencies were better determined by special tests when components were perturbed from their normal operational conditions than by any sort of regression technique on operational data. Generally the instrument was better operated asynchronously with orbit so that orbital effects were more easily identified. Some ISAMS channels had about 22 radiometric calibration sequences per orbit which was adequate (when doing HIRDLS-like single-sided viewing) but the 6 calibration sequences used for some channels were not frequent enough to follow the observed variations in offset and gain during an orbit.

The optimal estimation techniques used to process Level 1 radiances to Level 2 (geophysical parameters such as temperature and volume mixing ratios) needed not only accurate radiance values but also reliable estimates of the radiance error terms in the "measurement error vector". On the ISAMS experiment it was found that the best error estimates could be derived from multiple repeated successive observations of the same variable over a short period of time. Simple pairs of adjacent observations were invaluable.

Validation of the radiometric calibration required that the radiometric performance of the instrument can be well-modelled. This demanded knowledge of the representative temperature and emissivities of all optical components. Emissivities are extremely difficult to measure in-orbit and only somewhat less so in a calibration facility. Not all the ISAMS mirror temperatures were telemetered and neither was that of the chopper. Consequently a full validation of the radiometric model was not possible. There was also some evidence that the telemetered temperature of the internal calibration target did not represent its effective temperature. This was probably because of the inappropriate electronic circuit design which was used for these sensors. Algorithm design should not preclude minor modifications to incorporate improvements and corrections derived from in-flight experience.

A significant source of error in the ISAMS radiometric calibration was the scan-dependent stray radiance (i.e. telemetered radiances that varied with the scan mirror position). No method of measuring this error source in the HIRDLS calibration facility has been devised. However, if in orbit the spacecraft attitude is changed so that the radiometer views space (assumed to be uniform zero radiance source) with a variety of scan mirror angles then the scan-dependent radiance can be estimated. Assumptions about how the scan-dependent radiance might vary with spacecraft attitude and time also have to be made. For ISAMS these assumptions were very speculative because measurements were only obtained during two UARS roll manoeuvres separated by a period of six months. Two operational details added further complications to the study of scan-dependent strays: the variation in the azimuth of the scan mirror during the measurements was synchronous with the orbit and also two different reference (calibration) views were used for the two spacecraft manoeuvres. However, there was evidence that ISAMS scan-stray radiances did not vary significantly with time or with spacecraft attitude. Nevertheless there were consistent significant differences between closely-related channels and detector elements so similarity between channels must not be assumed.

Although contamination of the instrument fields-of-view by radiation from non-atmospheric sources (principally the moon) was in practice a rare event it can be a significant source of error which may be overlooked because it tends to occur at the same observed latitude for a few orbits. It is therefore important that radiances known from ephemeris calculations to be contaminated are flagged as such. The geometry of the ISAMS space-reference port field-of-view was not measured and had to be estimated from instrument drawings.

Considerable effort was expended in the development of ISAMS algorithms to provide resilience against possible energetic particle events (particularly in the South Atlantic Anomaly) affecting the detector electronics and causing "spikes" in the radiance telemetry. In practice no radiance "spikes" were ever attributed to this cause but the micro-processor random access memory suffered several (reversible) single-bit corruptions.

Before UARS launch it was anticipated that the limiting factor in the use of ISAMS radiances would be the detector noise and this concept was implicitly incorporated in some algorithms. In practice it was found to be the detector gain (which between detector decontamination sequences was extremely closely related to detector temperature) was more of a performance limitation because of signal quantisation.

ISAMS production data processing software contained several components intended to provide data for monitoring instrument performance. Although this function is essential it is not clear that it is best combined with production processing.

It was found that some ISAMS data were unsuitable for production processing (for example during special observing sequences) and there was no easy way of determining this from the telemetry stream alone. A calibration file indicating the time span of data which should be avoided by production processing would have been better than the ad-hoc approach used.

Some problems in ISAMS processing were caused by calibration of the pressure modulators and molecular sieves. These components will not be used in HIRDLS. However ISAMS did not have gyroscopes attached to the optical bench nor did it operate over a wide azimuth scan.

3. CALIBRATION ALGORITHMS

3.1 RAW DATA QUALITY CONTROL

All algorithms must be designed to handle unexpected values in the data stream cleanly. Most common failures of this kind are caused by overflows (division by zero) and attempting to calculate the square root of negative numbers. On detection of such problems algorithms will issue warnings to the PI team and, where possible, flag a section of data as unreliable and continue to the next section. In all cases algorithms should terminate in a predictable fashion.

Inevitably some data will be corrupted in transmission from the satellite to the data processing facility. By judicious choice of protocols most of the errors will be detected and corrected in the Level 0 product. However, there will remain some data which should be flagged as corrupted and all processing algorithms must check this data quality information (e.g. parity errors, checksum errors, loss of synchronisation, drop-outs etc) to ensure that suspect information is not used in data processing.

Some items in the data stream follow simple patterns that should be checked for consistency. Typically there are counters which are expected to increment in a predictable way. There are a few cooler subsystem items where the mechanism telemetry can be checked against the mechanism demand. The action to be taken on detection of an anomaly needs to be determined on a case-by-case basis but invariably a detailed warning needs to be issued to the PI team.

Many temperatures, particularly those important in radiometric calibration, are measured with multiple sensors of different types (thermistors and platinum resistance thermometers). Large discrepancies between measurements which are expected to be similar will be monitored and reported to the PI team. Suspect telemetry values will not be used in calibration.

Some housekeeping telemetry is expected to vary smoothly (e.g. mirror temperatures) or be effectively constant (e.g. reference voltages) but may in practice exhibit spikes possibly caused by energetic particles affecting a sensor. Similar effects are also seen when working near the digitisation limit of an analog to digital convertor. In such cases a spike detection and removal algorithm is required. Because the data to be de-spiked are not necessarily evenly spaced in time, and because the filter has to be capable of fine tuning, a Kalman filter technique is particularly appropriate.

3.2 ENGINEERING TELEMETRY CONVERSION

A significant part of the test and calibration phase of HIRDLS will be the validation of the engineering telemetry conversion. Indeed it is planned that some of the same source code used for test and calibration will be used in the production data processing. Temperatures which are required to high precision (e.g. the IFC Black Body temperatures used in radiometric calibration) will be measured using 500 ohm platinum resistance sensors on a 4-wire AC bridge for which polynomial coefficients are provided to convert telemetered values to values on the International Temperature Scale. The following table lists all the data items which will be contained in the HIRDLS Level 0 (instrument telemetry) file and indicates, where appropriate, the algorithm used to convert each item into engineering units. Items used in the calibration algorithms described in this document are indicated by '+'.

MNEMONIC	DESCRIPTION	<u>ALGORITHM</u>	Chopper revs./ Sample ID
AZIMDAT	+ Azimuth encoder	tbd	1 103
AZMOTR_CRRT	Azimuth motor current	D	8 107
AZMOTTMP	Azimuth motor temperature	D	64 138
BEUBOXTMP	BEU box temperature	D	64 388
BEUMNTTMP	BEU mount temperature	D	64 389
CALMIRTMP01	+ Cal. Mirror temperature #1	D	64 150
CALMIRTMP02	+ Cal. Mirror temperature #2	D	64 151
CALMIRTMP03	+ Cal. Mirror temperature #3	ZC	64 152
CCUBOXTMP	CCU box temperature	D	64 37
CHOPSGTMP01	Chopper housing temperature #1	D	64 147
CHOPSGTMP02	Chopper housing temperature #2	D	64 148
CHOPSGTMP03	Chopper housing temperature #3	ZC	64 149
CHOPMOT_CRRT	Chopper motor current	tbd	64 112
CHOP_PERIOD	+ Chopper period setting	ZB	64 387
CMD_CSCI_BUILD_ID	Command S/W Build Version ID	none	64 323
COMPHEADTMP	Compressor head temperature	D	64 44
COMP_AMP_ACT	Compressor amplitude (actual)	N3	64 339
COMP_AMP_DMD	Compressor amplitude (demand)	N3	64 338
COOLRADTMP1	Cooler Radiator temperature 1	D	64 42
COOLRADTMP2	Cooler Radiator temperature 2	D	64 43
CRYOTIP_SETP	Cryo tip temperature set point	N1	64 331
CRYOTIP_TMP_D0	Cryo tip temperature 0	N1	64 332
CRYOTIP_TMP_D1	Cryo tip temperature 1	N1	64 333
CSS_CSCI_BUILD_ID	Cooler F/W Build Version ID	none	64 343
CSS_CURRENT	Cooler total mean current	M	64 330
CSS_DDCAG_STAT	Cooler DDC & caging status	none	64 328

CSS_ERROR	Cooler error flags	none	64	329
CSS_FREQ_ACT	Cooler frequency (actual)	P	64	335
CSS_FREQ_DMD	Cooler frequency (demand)	P	64	334
CSS_MSG_NUMBER	CSS-IPS data message number	none	64	342
CSS_OPSTATUS	Cooler operating status	none	64	327
CSS_PH_ACT	Comp./Disp. phase (actual)	N2	64	337
CSS_PH_DMD	Comp./Disp. phase demand)	N2	64	336
DISPL1TMP	Displacer 1 body temperature	D	64	45
DISPL2TMP	Displacer 2 body temperature	D	64	46
DISP_AMP_ACT	Displacer amplitude (actual)	N3	64	341
DISP_AMP_DMD	Displacer amplitude (demand)	N3	64	340
DOOR_POT	Door angle sensor	B	64	410
DOOR_SAF_ANG	Door Safe Angle setting	B	64	51
EEABOXTMP	EEA box temperature	D	64	40
EEAMNTTMP	EEA mount temperature	D	64	394
EEA_STATUS	EEA configuration status	none	64	104
ELEVDATA	+ Elevation encoder A	tbd	1	101
ELEVDATB	+ Elevation encoder B	tbd	1	102
ELMOT1TMP1	Elevation motor 1 temperature	1 D	64	395
ELMOT1TMP2	Elevation motor 1 temperature	2 D	64	396
ELMOT2TMP1	Elevation motor 2 temperature	1 D	64	397
ELMOT2TMP2	Elevation motor 2 temperature	2 D	64	397
ELMOTR1_CRRT	Elevation motor 1 current	D	8	105
ELMOTR2_CRRT	Elevation motor 2 current	D	8	106
FPA_TEMP_A	Focal Plane temperature A	tbd	64	163
FPA_TEMP_B	Focal Plane temperature B	tbd	64	164
FRAMECNT	Minor frame count	none	8	267
GEUBOXTMP	GEU box temperature	D	64	38
GMU_HSG_TMP	GMU Housing temperature	D	64	161
GMU_MNT_TMP	GMU Mount temperature	D	64	160
GYR0_ADAT	+ Gyro 0 angle data	Section 3.5	1	69
GYR0_BDTMP	+ Gyro 0 board temperature	tbd	64	65
GYR0_CAPL	Gyro 0 cap loop output	tbd	64	77
GYR0_MAGDAT	+ Gyro 0 magnetometer data	Section 3.5	64	73
GYR0_MOTC	Gyro 0 motor current	tbd	64	85
GYR0_MOTV	Gyro 0 motor volts	tbd	64	81
GYR0_N15V	Gyro 0 -15 volts	tbd	64	97
GYR0_P15V	Gyro 0 +15 volts	tbd	64	93
GYR0_STAT	Gyro 0 status word	none	64	89
GYR0_TEMP	+ Gyro 0 temperature	E	64	61
GYR1_ADAT	+ Gyro 1 angle data	Section 3.5	1	70
GYR1_BDTMP	+ Gyro 1 board temperature	tbd	64	66
GYR1_CAPL	Gyro 1 cap loop output	tbd	64	78
GYR1_MAGDAT	+ Gyro 1 magnetometer data	Section 3.5	64	74
GYR1_MOTC	Gyro 1 motor current	tbd	64	86
GYR1_MOTV	Gyro 1 motor volts	tbd	64	82
GYR1_N15V	Gyro 1 -15 volts	tbd	64	98
GYR1_P15V	Gyro 1 +15 volts	tbd	64	94
GYR1_STAT	Gyro 1 status word	none	64	90
GYR1_TEMP	+ Gyro 1 temperature	E	64	62
GYR2_ADAT	+ Gyro 2 angle data	Section 3.5	1	71
GYR2_BDTMP	+ Gyro 2 board temperature	tbd	64	67
GYR2_CAPL	Gyro 2 cap loop output	tbd	64	79
GYR2_MAGDAT	+ Gyro 2 magnetometer data	Section 3.5	64	75
GYR2_MOTC	Gyro 2 motor current	tbd	64	87
GYR2_MOTV	Gyro 2 motor volts	tbd	64	83
GYR2_N15V	Gyro 2 -15 volts	tbd	64	99
GYR2_P15V	Gyro 2 +15 volts	tbd	64	95
GYR2_STAT	Gyro 2 status word	none	64	91
GYR2_TEMP	+ Gyro 2 temperature	E	64	63
GYR3_ADAT	+ Gyro 3 angle data	Section 3.5	1	72
GYR3_BDTMP	+ Gyro 3 board temperature	tbd	64	68
GYR3_CAPL	Gyro 3 cap loop output	tbd	64	80
GYR3_MAGDAT	+ Gyro 3 magnetometer data	Section 3.5	64	76

GYR3_MOTC	Gyro 3 motor current	tbd	64	88
GYR3_MOTV	Gyro 3 motor volts	tbd	64	84
GYR3_N15V	Gyro 3 -15 volts	tbd	64	100
GYR3_P15V	Gyro 3 +15 volts	tbd	64	96
GYR3_STAT	Gyro 3 status word	none	64	92
GYR3_TEMP	+ Gyro 3 temperature	E	64	64
HIRCLKLSB	HIRDLS clock least sig. byte	none	1	251
HK_FORMAT_ID	Housekeeping format table ID	none	8	268
IFCBB_FRPL_TMP	IFCBB front plate temperature	tbd	64	165
IFCBB_TMP1	+ IFC Black Body temperature #1	K1	64	167
IFCBB_TMP2	+ IFC Black Body temperature #2	K2	64	168
IFCBB_TMP3	+ IFC Black Body temperature #3	K3	64	169
IFC_OVEN_TMP	IFC ref resistor oven temp	L	64	166
IFC_PSV_N15	IFC -15V rail volts	H	64	172
IFC_PSV_P15	IFC +15V rail volts	G	64	171
IFC_PSV_P28	IFC +28V rail volts	F	64	170
IFC_PSV_P5	IFC +5V rail volts	J	64	173
IPUBOXTMP	IPU box temperature	D	64	391
IPU_3P3DDC_TMP	Wkg IPU +3.3V DDC temperature	D	64	304
IPU_3P3VOLTS	Wkg IPU +3.3V supply volts	W	64	300
IPU_5VDDC_TMP	Wkg IPU +5V DDC temperature	D	64	305
IPU_5VOLTS	Wkg IPU +5V supply volts	V	64	301
IPU_CSCI_BUILD_ID	IPU S/W Build Version ID	none	64	325
IPU_N15VOLTS	Wkg IPU -15V supply volts	X2	64	303
IPU_P15VOLTS	Wkg IPU +15V supply volts	X1	64	302
LNS1WFTMP01	+ Lens 1-WF temperature 1	D	64	141
LNS1WFTMP02	+ Lens 1-WF temperature 2	D	64	142
LNS1WFTMP03	+ Lens 1-WF temperature 3	ZC	64	143
LNS2TMP01	+ Lens 2 temperature 1	D	64	144
LNS2TMP02	+ Lens 2 temperature 2	D	64	145
LNS2TMP03	+ Lens 2 temperature 3	ZC	64	146
LNSASSY_TMP01	OBA lens assembly temp. #1	D	64	156
LNSASSY_TMP02	OBA lens assembly temp. #2	D	64	157
M1TMP01	Pri. (M1) mirror temperature 1	D	64	139
M1TMP02	Pri. (M1) mirror temperature 2	D	64	140
M1TMP03	Pri. (M1) mirror temperature 3	ZC	64	399
M2TMP01	Sec. (M2) mirror temperature #1	D	64	153
M2TMP02	Sec. (M2) mirror temperature #2	ZC	64	154
MACMDS_RCVCT	Macro commands: received count	none	64	263
MACMDS_REJCT	Macro cmds: rejected count	none	64	264
MACMD_LAST_CN	Last Macro command: number	none	64	266
MACMD_LAST_RC	Last Macro command: result code	none	64	265
OBA_PLT_TMP	OBA aperture plate temp	D	64	159
ORB_DAT_00	S/C Ancillary data item #0	tbd	64	21
ORB_DAT_01	S/C Ancillary data item #1	tbd	64	22
ORB_DAT_02	S/C Ancillary data item #2	tbd	64	23
ORB_DAT_03	S/C Ancillary data item #3	tbd	64	24
ORB_DAT_04	S/C Ancillary data item #4	tbd	64	25
ORB_DAT_05	S/C Ancillary data item #5	tbd	64	26
ORB_DAT_06	S/C Ancillary data item #6	tbd	64	27
ORB_DAT_07	S/C Ancillary data item #7	tbd	64	28
PCUBOXTMP	PCU box temperature	D	64	39
PSS_PCU_15VATMP	PCU (Internal) 15VA DDC temp.	ZA	64	383
PSS_PCU_15VBTMP	PCU (Internal) 15VB DDC temp.	ZA	64	384
PSS_PCU_5V	PCU Internal +5 Volts	R	64	352
PSS_PCU_N15V	PCU Internal -15 Volts	S2	64	354
PSS_PCU_P15V	PCU Internal +15 Volts	S1	64	353
PSS_QAFILT_TMP	PCU QBA Inrush Filter temp.	ZA	64	385
PSS_QBFILT_TMP	PCU QBB Inrush Filter temp.	ZA	64	386
PSS_REG_28VA	REG +28V DDC A volts	U4	64	355
PSS_REG_28VATMP	REG +28VA DDC temperature	ZA	64	375
PSS_REG_28VB	REG +28V DDC B volts	U4	64	356
PSS_REG_28VBTMP	REG +28VB DDC temperature	ZA	64	376
PSS_SPU_15VATMP	SPU 15VA DDC temperature	ZA	64	373

PSS_SPU_15VBTMP	SPU 15VB DDC temperature	ZA	64 374
PSS_SPU_5VA	SPU +5V DDC A volts	U1	64 346
PSS_SPU_5VATMP	SPU +5VA DDC temperature	ZA	64 371
PSS_SPU_5VB	SPU +5V DDC B volts	U1	64 347
PSS_SPU_5VBTMP	SPU +5VB DDC temperature	ZA	64 372
PSS_SPU_N15VA	SPU -15V DDC A volts	U3	64 350
PSS_SPU_N15VB	SPU -15V DDC B volts	U3	64 351
PSS_SPU_P15VA	SPU +15V DDC A volts	U2	64 348
PSS_SPU_P15VB	SPU +15V DDC B volts	U2	64 349
PSS_STATUS_00	PSS relay status word 0	none	64 363
PSS_STATUS_01	PSS relay status word 1	none	64 364
PSS_STATUS_02	PSS relay status word 2	none	64 365
PSS_STATUS_03	PSS relay status word 3	none	64 366
PSS_STATUS_04	PSS relay status word 4	none	64 367
PSS_STATUS_05	PSS relay status word 5	none	64 368
PSS_STATUS_06	PSS relay status word 6	none	64 369
PSS_STATUS_07	PSS relay status word 7	none	64 370
PSS_SYS_5VA	SYS +5V DDC A volts	U1	64 357
PSS_SYS_5VATMP	SYS +5VA DDC temperature	ZA	64 377
PSS_SYS_5VB	SYS +5V DDC B volts	U1	64 358
PSS_SYS_5VBTMP	SYS +5VB DDC temperature	ZA	64 378
PSS_SYS_N15VA	SYS -15V DDC A volts	U3	64 361
PSS_SYS_N15VATMP	SYS -15VA DDC temperature	ZA	64 381
PSS_SYS_N15VB	SYS -15V DDC B volts	U3	64 362
PSS_SYS_N15VBTMP	SYS -15VB DDC temperature	ZA	64 382
PSS_SYS_P15VA	SYS +15V DDC A volts	U2	64 359
PSS_SYS_P15VATMP	SYS +15VA DDC temperature	ZA	64 379
PSS_SYS_P15VB	SYS +15V DDC B volts	U2	64 360
PSS_SYS_P15VBTMP	SYS +15VB DDC temperature	ZA	64 380
QBA_CURRT	Quiet Bus A input current	tbd	64 344
QBB_CURRT	Quiet Bus B input current	tbd	64 345
SAILCMDST_0_31	SAIL command attributes Status	none	64 230
SAILCMDST_32_63	SAIL command attributes Status	none	64 231
SAILCMDST_64_95	SAIL command attributes Status	none	64 232
SAILCMDST_96_127	SAIL command attributes Status	none	64 233
SAILTASK00_HI	SAIL Task 0 parameters 8-15	none	8 175
SAILTASK00_LO	SAIL Task 0 parameters 0-7	none	8 174
SAILTASK01_HI	SAIL Task 1 parameters 8-15	none	8 177
SAILTASK01_LO	SAIL Task 1 parameters 0-7	none	8 176
SAILTASK02_HI	SAIL Task 2 parameters 8-15	none	8 179
SAILTASK02_LO	SAIL Task 2 parameters 0-7	none	8 178
SAILTASK03_HI	SAIL Task 3 parameters 8-15	none	8 181
SAILTASK03_LO	SAIL Task 3 parameters 0-7	none	8 180
SAILTASK04_HI	SAIL Task 4 parameters 8-15	none	8 183
SAILTASK04_LO	SAIL Task 4 parameters 0-7	none	8 182
SAILTASK05_HI	SAIL Task 5 parameters 8-15	none	8 185
SAILTASK05_LO	SAIL Task 5 parameters 0-7	none	8 184
SAILTASK06_HI	SAIL Task 6 parameters 8-15	none	8 187
SAILTASK06_LO	SAIL Task 6 parameters 0-7	none	8 186
SAILTASK07_HI	SAIL Task 7 parameters 8-15	none	8 189
SAILTASK07_LO	SAIL Task 7 parameters 0-7	none	8 188
SAILTASK08_HI	SAIL Task 8 parameters 8-15	none	8 191
SAILTASK08_LO	SAIL Task 8 parameters 0-7	none	8 190
SAILTASK09_HI	SAIL Task 9 parameters 8-15	none	8 193
SAILTASK09_LO	SAIL Task 9 parameters 0-7	none	8 192
SAILTASK10_HI	SAIL Task 10 parameters 8-15	none	8 195
SAILTASK10_LO	SAIL Task 10 parameters 0-7	none	8 194
SAILTASK11_HI	SAIL Task 11 parameters 8-15	none	8 197
SAILTASK11_LO	SAIL Task 11 parameters 0-7	none	8 196
SAILTASK12_HI	SAIL Task 12 parameters 8-15	none	8 199
SAILTASK12_LO	SAIL Task 12 parameters 0-7	none	8 198
SAILTASK13_HI	SAIL Task 13 parameters 8-15	none	8 201
SAILTASK13_LO	SAIL Task 13 parameters 0-7	none	8 200
SAILTASK14_HI	SAIL Task 14 parameters 8-15	none	8 203

SAILTASK14_LO	SAIL Task 14 parameters 0-7	none	8	202
SAILTASK15_HI	SAIL Task 15 parameters 8-15	none	8	205
SAILTASK15_LO	SAIL Task 15 parameters 0-7	none	8	204
SAILTSKSTAT_00	SAIL Task 0 Status Code	none	64	235
SAILTSKSTAT_01	SAIL Task 1 Status Code	none	64	236
SAILTSKSTAT_02	SAIL Task 2 Status Code	none	64	237
SAILTSKSTAT_03	SAIL Task 3 Status Code	none	64	238
SAILTSKSTAT_04	SAIL Task 4 Status Code	none	64	239
SAILTSKSTAT_05	SAIL Task 5 Status Code	none	64	240
SAILTSKSTAT_06	SAIL Task 6 Status Code	none	64	241
SAILTSKSTAT_07	SAIL Task 7 Status Code	none	64	242
SAILTSKSTAT_08	SAIL Task 8 Status Code	none	64	243
SAILTSKSTAT_09	SAIL Task 9 Status Code	none	64	244
SAILTSKSTAT_10	SAIL Task 10 Status Code	none	64	245
SAILTSKSTAT_11	SAIL Task 11 Status Code	none	64	246
SAILTSKSTAT_12	SAIL Task 12 Status Code	none	64	247
SAILTSKSTAT_13	SAIL Task 13 Status Code	none	64	248
SAILTSKSTAT_14	SAIL Task 14 Status Code	none	64	249
SAILTSKSTAT_15	SAIL Task 15 Status Code	none	64	250
SAIL_CSCI_BUILD_ID	SAIL S/W Build Version ID	none	64	326
SAIL_PROC_STAT	SAIL Processor Status Code	none	64	234
SAIL_SHM_504	SAIL shared memory [504]	none	64	222
SAIL_SHM_505	SAIL shared memory [505]	none	64	223
SAIL_SHM_506	SAIL shared memory [506]	none	64	224
SAIL_SHM_507	SAIL shared memory [507]	none	64	225
SAIL_SHM_508	SAIL shared memory [508]	none	64	226
SAIL_SHM_509	SAIL shared memory [509]	none	64	227
SAIL_SHM_510	SAIL shared memory [510]	none	64	228
SAIL_SHM_511	SAIL shared memory [511]	none	64	229
SCAN_BASE_TMP	OBA Scanner base temperature	D	64	155
SCAN_MOT_STAT	Scan Mirror drive motor status	none	64	117
SCCMDS_RCVCT	S/C commands: received count	none	64	254
SCCMDS_REJCT	S/C commands: rejected count	none	64	255
SCCMD_LAST_CN	Last S/C cmd: command number	none	64	257
SCCMD_LAST_PC	Last S/C cmd: packet seq. count	none	64	258
SCCMD_LAST_RC	Last S/C command: result code	none	64	256
SIG_DAT_01	+ Radiance channel 1	Section 3.8	1	0
SIG_DAT_02	+ Radiance channel 2	Section 3.8	1	1
SIG_DAT_03	+ Radiance channel 3	Section 3.8	1	2
SIG_DAT_04	+ Radiance channel 4	Section 3.8	1	3
SIG_DAT_05	+ Radiance channel 5	Section 3.8	1	4
SIG_DAT_06	+ Radiance channel 6	Section 3.8	1	5
SIG_DAT_07	+ Radiance channel 7	Section 3.8	1	6
SIG_DAT_08	+ Radiance channel 8	Section 3.8	1	7
SIG_DAT_09	+ Radiance channel 9	Section 3.8	1	8
SIG_DAT_10	+ Radiance channel 10	Section 3.8	1	9
SIG_DAT_11	+ Radiance channel 11	Section 3.8	1	10
SIG_DAT_12	+ Radiance channel 12	Section 3.8	1	11
SIG_DAT_13	+ Radiance channel 13	Section 3.8	1	12
SIG_DAT_14	+ Radiance channel 14	Section 3.8	1	13
SIG_DAT_15	+ Radiance channel 15	Section 3.8	1	14
SIG_DAT_16	+ Radiance channel 16	Section 3.8	1	15
SIG_DAT_17	+ Radiance channel 17	Section 3.8	1	16
SIG_DAT_18	+ Radiance channel 18	Section 3.8	1	17
SIG_DAT_19	+ Radiance channel 19	Section 3.8	1	18
SIG_DAT_20	+ Radiance channel 20	Section 3.8	1	19
SIG_DAT_21	+ Radiance channel 21	Section 3.8	1	20
SIG_ZERO_01	+ Channel 1 Zero Offset	none	64	269
SIG_ZERO_02	+ Channel 2 Zero Offset	none	64	270
SIG_ZERO_03	+ Channel 3 Zero Offset	none	64	271
SIG_ZERO_04	+ Channel 4 Zero Offset	none	64	272
SIG_ZERO_05	+ Channel 5 Zero Offset	none	64	273
SIG_ZERO_06	+ Channel 6 Zero Offset	none	64	274
SIG_ZERO_07	+ Channel 7 Zero Offset	none	64	275

SIG_ZERO_08	+ Channel 8 Zero Offset	none	64 276
SIG_ZERO_09	+ Channel 9 Zero Offset	none	64 277
SIG_ZERO_10	+ Channel 10 Zero Offset	none	64 278
SIG_ZERO_11	+ Channel 11 Zero Offset	none	64 279
SIG_ZERO_12	+ Channel 12 Zero Offset	none	64 280
SIG_ZERO_13	+ Channel 13 Zero Offset	none	64 281
SIG_ZERO_14	+ Channel 14 Zero Offset	none	64 282
SIG_ZERO_15	+ Channel 15 Zero Offset	none	64 283
SIG_ZERO_16	+ Channel 16 Zero Offset	none	64 284
SIG_ZERO_17	+ Channel 17 Zero Offset	none	64 285
SIG_ZERO_18	+ Channel 18 Zero Offset	none	64 286
SIG_ZERO_19	+ Channel 19 Zero Offset	none	64 287
SIG_ZERO_20	+ Channel 20 Zero Offset	none	64 288
SIG_ZERO_21	+ Channel 21 Zero Offset	none	64 289
SLCMDS_RCVCT	SAIL commands: received count	none	64 259
SLCMDS_REJCT	SAIL commands: rejected count	none	64 260
SLCMD_LAST_CN	Last SAIL command: number	none	64 262
SLCMD_LAST_RC	Last SAIL command: result code	none	64 261
SMTMP01	Scan mirror temperature 1	D	64 133
SMTMP02	Scan mirror temperature 2	D	64 134
SMTMP03	Scan mirror temperature 3	ZC	64 135
SPUBOXTMP	SPU box temperature	D	64 390
SPU_N12VOLTS_A	SPU -12VA supply volts	ZE2	64 294
SPU_N12VOLTS_B	SPU -12VB supply volts	ZE2	64 299
SPU_N5VOLTS_A	SPU -5VA supply volts (analog)	ZD2	64 291
SPU_N5VOLTS_B	SPU -5VB supply volts (analog)	ZD2	64 296
SPU_P12VOLTS_A	SPU +12VA supply volts	ZE1	64 293
SPU_P12VOLTS_B	SPU +12VB supply volts	ZE1	64 298
SPU_P5VOLTS_A	SPU +5VA supply volts (analog)	ZD1	64 290
SPU_P5VOLTS_B	SPU +5VB supply volts (analog)	ZD1	64 295
SPU_P5VOLTS_DA	SPU +5VA supply volts (digital)	ZD1	64 292
SPU_P5VOLTS_DB	SPU +5VB supply volts (digital)	ZD1	64 297
SPVUMIRTMP1	Space View Mirror temperature 1	D	64 400
SPVUMIRTMP1	Space View Mirror temperature 2	D	64 401
SPVUMIRTMP1	Space View Mirror temperature 3	ZC	64 402
SPVU_BAF_TMP	OBA Space View baffle tmp	D	64 158
SSHWA_TMP	Hot Wax Actuator temperature	C	64 52
SSH_APL_TMP	SSH aperture plate temperature	D	64 54
SSH_DORMOT_TMP	SSH drive motor temperature	C	64 53
SSH_NZSURF_TMP	SSH -Z surface temperature	D	64 56
SSH_PZSURF_TMP	SSH +Z surface temperature	D	64 55
SSH_STATUS	Sunshield switch status	none	64 57
STH_TMP_01	Structure temperature 1	D	64 29
STH_TMP_02	Structure temperature 2	D	64 30
STH_TMP_03	Structure temperature 3	D	64 31
STH_TMP_04	Structure temperature 4	D	64 32
SUNSEN1_TMP	Sun sensor 1 (temperature)	A	64 47
SUNSEN2_TMP	Sun sensor 2 (temperature)	A	64 48
SUNSEN3_TMP	Sun sensor 3 (temperature)	A	64 49
SVA_DORMOT_TMP	SVA drive motor temperature	C	64 59
SVA_MTGPLT_TMP	SVA mounting plate temperature	D	64 60
SVA_STATUS	SVA switch status	none	64 58
TEUBOXTMP	TEU box temperature	D	64 392
TEUMNTTMP	TEU mount temperature	D	64 393
TEU_ADC0_REF	TEU ADC0 +5V ref. volts	tbd	64 118
TEU_ADC0_ZER	TEU ADC0 +5V zero volts	tbd	64 122
TEU_ADC1_REF	TEU ADC1 +5V ref. volts	tbd	64 119
TEU_ADC1_ZER	TEU ADC1 +5V zero volts	tbd	64 123
TEU_ADC2_REF	TEU ADC2 +5V ref. volts	tbd	64 120
TEU_ADC2_ZER	TEU ADC2 +5V zero volts	tbd	64 124
TEU_ADC3_REF	TEU ADC3 +5V ref. volts	tbd	64 121
TEU_ADC3_ZER	TEU ADC3 +5V zero volts	tbd	64 125
TEU_N9V	TEU -9V rail voltage	tbd	64 128
TEU_P5V	TEU +5V rail voltage	tbd	64 126

TEU_P9V	TEU +9V rail voltage	tbd	64	127
TEU_SIGCON_STAT	TEU Signal Cond Data Acq status	none	64	116
TEU_STATUS	TEU Processor Config. status	none	64	114
TEU_TSW_STAT	Telescope S/W Status	none	64	113
TLM_CSCI_BUILD_ID	Telemetry S/W Build Version ID	none	64	324
TMARK_CLK	Time Mark clock word	none	64	252
TMARK_DATA	Time mark data word	none	64	253
TSS_HW_CFIG	TSS hardware configuration	none	64	115
TSW_CSCI_BUILD_ID	Telescope S/W Build Version ID	none	64	162
WOBB_SENS1	+ Wobble sensor 1 data		64	108
WOBB_SENS2	+ Wobble sensor 2 data		64	109
WSEBOXTMP	WSE box temperature	D	64	41

CONVERSION ALGORITHMS

Three types of function are used for engineering conversion: polynomial, logarithmic and reciprocal.

Polynomial, P, conversions are of the form

$$p = c_0 + c_1(n-h) + c_2(n-h)^2 + c_3(n-h)^3 + \dots$$

where

n is the raw telemetry counts

h is the half scale offset (included in formulation for numerical precision)

c_i are the polynomial coefficients

Logarithmic, L, conversions are of the form

$$p = c_0 + c_1 \ln(n)$$

where

n is the raw telemetry counts

c_i are specified coefficients

Reciprocal, R, conversions are of the form

$$p = c_0 / (n + c_1)$$

where

n is the raw telemetry counts

c_i are specified coefficients

Alg.	Type	Coef.	h	Units	Used for
A				C	Sun Sensors
B	P	2	32768	degrees	Sunshield door potentiometer
C	P	2	32768	K	AD590
D	P	2	32768	K	Matrix AD590s
E				C	Gyro motor temperature
F	P	2	128	volts	IFC +28V
G	P	2	128	volts	IFC +15V
H	P	2	128	volts	IFC -15V
J	P	2	128	volts	IFC +5V
K1A	P	6	32768	K	IFC Black Body Temperature #1A

K2A	P	6	32768	K	IFC Black Body Temperature #2A
K3A	P	6	32768	K	IFC Black Body Temperature #3A
K1B	P	6	32768	K	IFC Black Body Temperature #1B
K2B	P	6	32768	K	IFC Black Body Temperature #2B
K3B	P	6	32768	K	IFC Black Body Temperature #3B
L	L			C	IFC Ref. Resistor Oven Temperature
M	P	2	128	amps	Cooler subsystem current
N1	P	2	32768	K	Cryo temperatures
N2	P	2	32768	degrees	Cooler phase angle
N3	P	2	32768	%	Cooler stroke amplitude
P	P	2	128	Hz	Cooler frequency
R	P	2	32768	volts	+5V internal power supply
S1	P	2	32768	volts	+15V internal power supply
S2	P	2	32768	volts	-15V internal power supply
U1	P	2	32768	volts	+5V power supply
U2	P	2	32768	volts	+15V power supply
U3	P	2	32768	volts	-15V power supply
U4	P	2	32768	volts	28V power supply
V	P	2	32768	volts	Processor +5V
W	P	2	32768	volts	Processor +3.3V
X1	P	2	32768	volts	Processor +15V
X2	P	2	32768	volts	Processor -15V
ZA	P	2	32768	C	PCU temperatures
ZB	R			Hz	Chopper period
ZC	P	2	32768	C	Optical bench PRTs
ZD1	P	2	32768	volts	Signal Processing Unit +5V
ZD2	P	2	32768	volts	Signal Processing Unit -5V
ZE1	P	2	32768	volts	Signal Processing Unit +12V
ZE2	P	2	32768	volts	Signal Processing Unit -12V

3.3 SPACECRAFT LOCATION

It is anticipated that the SDP Toolkit will be used to provide the definitive spacecraft latitude, longitude and altitude and ECI location at any time. The routine PGS_EPH_EphemAttit together with coordinate system conversion transformation tools (PGS_CSC_ECItoECR and PGS_CSC_ECRtoGEO) provide the necessary functionality. For testing and predictive purposes spacecraft location information can be generated from knowledge of the Keplerian orbital components and a model of the shape of the earth. A standard ellipsoid shape is adequate for HIRDLS Level 1 purposes.

3.4 SPACECRAFT ATTITUDE

The SDP Toolkit routine PGS_EPH_EphemAttit returns the spacecraft attitude (roll, pitch and yaw) at any specified time. This information will have been derived from the spacecraft gyroscope information and star sensors.

3.5 INSTRUMENT POINTING

To realise the full scientific potential of HIRDLS more accurate pointing information is needed than that provided by the spacecraft location and spacecraft attitude data and rigid body geometry alone. The optical system is mounted on a separate optical bench. There will inevitably be small time-varying distortions between the optical bench and the instrument baseplate and between the instrument baseplate and the spacecraft altitude measurement system. Consequently a set of rate-integrating gyroscopes is mounted on the optical bench to measure its orientation

continuously.

3.5.1 HIRDLS gyroscope calibration

Calibration of the HIRDLS gyroscope data and the use of this data in the accurate determination of instrument pointing is an extremely important issue for the data processing algorithms. The gyro subsystem generates telemetry (items GYR... in the Table in Section 3.2) on temperatures, voltages, currents, magnetic fields and rotation rates. Because the calibrations are interdependent they must be made in a specific order.

1. Gyro temperatures (GYRn_TEMP, GYRn_BDTEMP) to physical units (K).

These are converted and smoothed in the same way as other engineering data shown in Section 3.2. Converted values in the following discussion are indicated by a preceding 'c'. e.g. cGYRn_TEMP.

2. Magnetometer counts (GYRn_MAGDAT) to magnetic field in physical units (Tesla).

For each sensor, (n=1,2,3,4), define a signal offset corresponding to a zero field

$$C0_n = a_0 + a_1(cGYRn_TEMP - Tm_n) + a_2(cGYRn_BDTEMP - Te_n)$$

where Tm_n , Te_n are nominal operating temperatures and a_i , $i=0,2$, are constant coefficients measured prior to launch.

For $i=1,m$ ($m<4$), define scaling factors

$$b_{in} = f_{in} + g_{in}(cGYRn_TEMP - Tm_n) + h_{in}(cGYRn_BDTEMP - Te_n)$$

where f_{in} , g_{in} and h_{in} are coefficients measured prior to launch.

The magnetic field is then expressed as

$$\begin{aligned} B_n = & b_{1n}(GYRn_MAGDAT - C0_n) + \\ & b_{2n}(GYRn_MAGDAT - C0_n)^2 + \\ & b_{3n}(GYRn_MAGDAT - C0_n)^3 + \\ & \dots + \\ & b_{mn}(GYRn_MAGDAT - C0_n)^m \end{aligned}$$

Gyro angle uncalibrated rate determination

The gyro angle data for each chopper revolution (approximately 12ms) is contained as a signed integer in the ten least-significant-bits of the telemetry items GYRn_ADAT, $n=1,4$. We denote these values GYRn_ANG, $n=1,4$. The gyro uncalibrated rate (angle per unit time), gyrorateraw, is the difference between the gyro angle in the current chopper revolution, j , and the gyro angle in the previous revolution, $j-1$.

$$\text{gyrorateraw}_n(j) = (GYRn_ANG(j) - GYRn_ANG(j-1)) / cCHOP_PERIOD$$

In the event of data dropouts it should be possible to linearly-interpolate gyro angle to fill in missing values subject to the conditions that the time interval is less than 65 (tbv) chopper revolutions and that the total change in gyro angle is less than 256 (tbv). Note that it will be necessary to sum the rates within one elevation scan (profile) so all the

values of gyrorate within a profile will be needed.

Gyro rate correction for magnetic field and temperature and conversion to physical units.

The corrected gyro rate for each chopper revolution, gyrorate, is given by

$$\text{gyrorate}_n = \text{Sf}_n (\text{gyrorateraw}_n + \text{Cg}_n \text{B}_n + \text{Ct}_{1n}(\text{cGYRn_TEMP}-\text{Tm}_n) \\ + \text{Ct}_{2n}(\text{cGYRn_BDTEMP}-\text{Te}_n))$$

where scale factor Sf_n , magnetic field scale factor Cg_n , temperature sensitivity scale factors Ct_{1n} and Ct_{2n} are input calibration data constants for each of the four gyros.

3.5.2 Preliminary gyroscope trend correction

Definitive descriptions of the TRCF and IRCF coordinate reference frames are give in the [Instrument Technical Specification](#), (SP-HIR-013, ITS Section 3.13).

This trend correction is denoted preliminary because a more sophisticated procedure will be used for derivation of geopotential height gradients; the values generated here will be used for Level-2 retrieval, for which high relative precision within a profile is sufficient.

Let the gyro input axis vector in the Telescope Reference Coordinate Frame (TRCF) be \mathbf{V}_g . This is projected onto the ECI frame as follows :-

Let \mathbf{R}_{TI} be the direction cosine matrix specifying the TRCF in terms of the Instrument Reference Coordinate Frame (IRCF), including misalignments. \mathbf{R}_{TI} will be constant calibration data input.

Let \mathbf{R}_{IS} be the direction cosine matrix specifying the IRCF in terms of the spacecraft frame of reference (SFR), including misalignments. (Here, the SFR is a frame fixed physically in the spacecraft and independent of the orbit velocity vector). \mathbf{R}_{IS} will be constant calibration data input.

Let \mathbf{R}_{SE} be direction cosine matrix specifying the spacecraft frame (SFR) in terms of the ECI frame, including misalignments. \mathbf{R}_{SE} will vary continuously and is expected to be obtained from the SDP Toolkit routine PGS_EPH_EphemAttit.

The gyro vector in the ECI frame is now given by

$$\mathbf{V}_{gE} = \mathbf{R}_{SE} * \mathbf{R}_{IS} * \mathbf{R}_{TI} * \mathbf{V}_{gT}$$

The resolved rate, rateres, is now given by the rate of rotation of the SFR about this vector.

For the longest available period of high precision gyro operation for the axis in question (see note below), calculate

$$\text{rateav} = \text{Mean} \{ \text{rateres-gyrorate} \}$$

For computational efficiency it should not be necessary to use every value of rateres (one per chopper revolution). Use of one value every 64 chopper revolutions is acceptable. Data dropouts are permitted during this period but the average should only be performed over chopper revolutions for which gyrorate has been calculated. Each value of gyrorate (one per chopper revolution) over the period can now be corrected

$$\text{gyroratec}(j) = \text{gyrorate}(j) + \text{rateav}$$

Note: *Although individual gyros will in general have different periods of high precision*

operation, normally a given set of 3 gyros should operate for many days in high precision mode. However, the processing algorithm must be capable of processing blocks of data which includes gyro mode changes.

3.5.3 Integration of gyroscope angle within a profile

The derivation of calibrated and trend-corrected rates for each gyro unit has been described in sections 3.5.1 and 3.5.2. where each gyro unit was treated separately. It is now necessary to integrate these rates and combine them to describe the motion of the optical bench. The retrieval process requires high accuracy of the relative elevation angle or tangent height between different samples that comprise a single elevation scan. Consequently the approach adopted will be to constrain the attitude to agree with the attitude provided by the SDP Toolkit at a single point in each elevation scan and to use the trend-corrected gyro rates to derive the attitude at other points. The process will generate the direction cosine matrix in the ECI frame, \mathbf{R}_{TE} , of the TRCF axes for each chopper revolution of the sequence as follows :-

1. Identify each section of data over which the gyro-derived attitude will be normalised to the Toolkit data. For baseline mode, and other conventional scanning modes, this section will be a single elevation profile of typically 10 seconds duration. For unusual modes (e.g. gravity wave modes where azimuth motions are tightly coupled with elevation movements), identification of a single sequence may not be straightforward. To assist with identification it may be assumed that the onboard SAIL task controlling scanning will identify each separate section (e.g. by a counter which changes at each sequence change).

If a set of three gyros do not provide good data throughout the section, instrument pointing correction using gyro data will not be possible. In this case the tangent point altitude data has to be derived from the Toolkit alone and must be flagged as such.

Select a chopper revolution as the integration starting point (e.g. the first, last or middle frame). This choice can be specified in calibration input data.

For the selected initial chopper revolution obtain from the Toolkit routine PGS_EPH_EphemAttit the SFR in the ECI frame (\mathbf{R}_{SE}).

2. Compute TRCF direction cosines in the ECI frame \mathbf{R}_{TE} for this time:

$$\mathbf{R}_{TE} = \mathbf{R}_{SE} * \mathbf{R}_{IS} * \mathbf{R}_{TI}$$

Integrate out from this point in time, forwards and/or backwards as necessary as follows, updating \mathbf{R}_{TE} each chopper revolution:

For each active gyro axis compute input axis vector \mathbf{V}_{gE} in the ECI frame

$$\mathbf{V}_{gE} = \mathbf{R}_{TE} * \mathbf{V}_{gT}$$

From the gyroratec values for the three active gyros compute the rotation during one chopper revolution, j , in the ECI reference frame (note that the gyros will not in general be orthogonal to each other). Apply this rotation to $\mathbf{R}_{TE}(j)$ to obtain $\mathbf{R}_{TE}(j+1)$ or $\mathbf{R}_{TE}(j-1)$ depending on integration direction. For forward integration $\mathbf{R}_{TE}(j)$ is obtained from $\mathbf{R}_{TE}(j-1)$ and gyroratec(j). For backward integration $\mathbf{R}_{TE}(j-1)$ is obtained from $\mathbf{R}_{TE}(j)$ and gyroratec(j) which is consistent with the rate definition assumed in section 3.5.1.

The end result is the orientation of the optical bench frame in the ECI frame, \mathbf{R}_{TE} , at every chopper revolution for the whole of the section of data (typically a single elevation scan).

3.5.4 Classification of instrument view type

In addition to the accurate determination of the true instrument pointing it is necessary to determine if the target is a valid atmospheric, space or black body view. Some radiances will have to be flagged as invalid for a variety of reasons e.g.

obstruction by sunshield door

warm detector elements

unreliable or unavailable telemetry data used in the pointing algorithm

obstruction in atmospheric or chopper reference view. See [Section 3.7](#)

3.6 CALCULATION OF LINE OF SIGHT DIRECTION AND TANGENT POINT LOCATION

So that the Level 1-2 processor can re-construct the accurate tangent point location (latitude, longitude and altitude) of each of the 21 detector elements it is necessary to include very precise information about the boresight vector and the rotation of the IFOV about the boresight in the Level 1 file. The derivation of this information is shown below. Further, the tangent point altitude of each detector element needs to be calculated for the Level 0-1 processor to decide if a view is a valid "space" view. Much less precision is required for this calculation. The SDP Toolkit routine PGS_CSC_GrazingRay will be used to determine the boresight tangent point and then constant altitude offsets for each row will be applied to this value. The tangent point location appropriate to each detector element will be determined using tabulated angular differences between the boresight and each detector.

3.6.1 Derivation of the optical train operator

For every chopper rotation an operator \mathbf{L} will be generated which rotates a vector in the TRCF entering and incident on the primary mirror to the corresponding line of sight direction in the ECIS frame incident upon the instrument. The ECIS frame is identical to the ECI frame except that it is instantaneously moving at the spacecraft velocity (the distinction is necessary to allow for aberration). Note that with the scan mirror in the nominal position and perfect geometry, the TRCF axes are parallel to the SFR axes, and that all rotation matrices denoted as corrections are unit matrices. For the actual instrument these will be precomputed and constant.

In this position the scan mirror normal would be along the $-X$ axis, which is along the $-velocity$ vector so a unit vector $(-1,0,0)$ represents the scan mirror normal. This is then rotated about the Y axis according to the selected calibrated elevation encoder angle ($elev[1]$ or $elev[2]$).

Rotation matrix, $\mathbf{R}_E =$

$$\begin{vmatrix} \cos(elev) & 0 & -\sin(elev) \\ 0 & 1 & 0 \\ \sin(elev) & 0 & \cos(elev) \end{vmatrix}$$

Apply the elevation gimbal correction rotation \mathbf{R}_{CE} to represent any misalignment of the elevation axis on its yoke (the axis should be normal to the azimuth axis, but prelaunch subsystem or instrument calibration will provide the precise orientation).

Rotate about the Z axis according to the calibrated azimuth encoder value ($azim$).

Rotation matrix, $\mathbf{R}_A =$

$$\begin{vmatrix} \cos(\text{azim}) & \sin(\text{azim}) & 0 \\ -\sin(\text{azim}) & \cos(\text{azim}) & 0 \\ 0 & 0 & 1 \end{vmatrix}$$

Apply azimuth gimbal correction rotation \mathbf{R}_{CA} to represent any misalignment of the azimuth axis (the axis should be parallel to the TRCF Z axis but prelaunch subsystem or instrument calibration will provide the precise orientation).

Apply the rotation correction matrix \mathbf{R}_W constructed from azimuth bearing wobble sensor calibrated values $w1 = \text{cWOBB_SENS1}[1]$ and $w2 = \text{cWOBB_SENS2}[2]$.

Rotation matrix, $\mathbf{R}_W =$

$$\begin{vmatrix} 1-w1*w1/2 & 0 & -w2 \\ 0 & 1-w2*w2/2 & w1 \\ w2 & -w1 & 1-(w1*w1+w2*w2)/2 \end{vmatrix}$$

(note that $w1$ and $w2$ are mechanically constrained to be very small angles of a few tens of microradians so that small angle approximations are valid).

The direction of the mirror normal in the TRCF is then given by the vector

$$\mathbf{V}_m = \mathbf{R}_W * \mathbf{R}_{CA} * \mathbf{R}_A * \mathbf{R}_{CE} * \mathbf{R}_E * (-1,0,0)$$

Next construct an operator \mathbf{M}_{REF} which will reflect vectors in a mirror of which \mathbf{V}_m is a normal. Apply \mathbf{R}_{TE} (derived in section 3.5) to transform to ECIS coordinates. We now have a rotation matrix $\mathbf{L} = \mathbf{R}_{TE} * \mathbf{M}_{REF}$ which takes a ray vector \mathbf{V} incident upon the instrument primary mirror (M1) and generates the corresponding line of sight view vector \mathbf{V}' incident on the scan mirror in the ECIS frame, i.e. $\mathbf{V}' = \mathbf{L} * \mathbf{V}$

3.6.2. Application to individual rays

We construct two ray vectors incident on the primary mirror (these will not vary so can be treated as constant calibration input data) :-

1. \mathbf{V}_b to represent the boresight. This has nominal direction cosines of $(-\cos(0.441568301), 0, -\sin(0.441568301))$. $[0.441568301 = 25.3 * \pi / 180]$. The as-built boresight direction will be determined during subsystem calibration.
2. \mathbf{V}_r arbitrarily taken to be directly 'above' the boresight on the focal plane at the elevation of the middle of the top row of detectors (channels 18,5 and 17). This angle is 8.934 mrad away from the boresight so the nominal direction cosines are $(-\cos(0.432634301), 0, -\sin(0.432634301))$. Again, the as-built vector will be derived during prelaunch calibration. \mathbf{V}_r will be used to calculate the apparent rotation of the IFOV about the boresight.

For each chopper revolution compute

$$\mathbf{V}_b' = \mathbf{L} * \mathbf{V}_b$$

where \mathbf{V}_b is the boresight vector in the ECIS frame. Transform to the ECI frame by correcting for aberration

$$\mathbf{V}_b'' = \text{Norm}\{\mathbf{V}_b' + (v_x, v_y, v_z)/c\}$$

where (v_x, v_y, v_z) is the satellite velocity vector in the ECI frame (obtained from PGS_EPH_EphemAttit), c is the velocity of light, and $\text{Norm}\{\}$ is the renormalisation function.

Use Toolkit routine PGS_CSC_GrazingRay together with \mathbf{V}_b'' and the scan mirror location in ECI coordinates (spacecraft location+scan mirror offset) to compute latitude, longitude and altitude and ECI location tp_eci of the boresight tangent point.

Use PGS_CSC_ECItOORBquat to obtain the ECI to Orbital Frame rotation quaternion and transform \mathbf{V}_b'' to Orbital frame coordinates \mathbf{V}_b''' .

Calculate the elevation angle,

$$\text{elevation} = \text{ARCCOS}(\mathbf{V}_b'''_z) \text{ (principal value)}$$

and the azimuth angle,

$$\text{azimuth} = \text{ARCTAN}(\mathbf{V}_b'''_y/\mathbf{V}_b'''_x) \text{ (principal value).}$$

Compute $\mathbf{V}_r' = \mathbf{L} * \mathbf{V}_r$ and transform to the ECI frame by correcting for aberration $\mathbf{V}_r'' = \text{Norm}\{\mathbf{V}_r' + (vx,vy,vz)/c\}$.

Finally, compute the rotation of IFOV relative to the boresight,

$$\text{field_rot} = \pi/2 - \text{ARCCOS}(\text{Norm}\{\mathbf{V}_r'' \times \mathbf{V}_b''\} \cdot \text{Norm}\{tp_eci\})$$

where \times denotes a cross product and \cdot a dot product. (The sign of bore_ray is TBV. The principal value is required). Note that the tp_eci is used here as a vector from the ECI origin.

3.6.3 Atmospheric Refraction

Atmospheric refraction due to air and water vapour are very significant for limb sounding, particularly below 30km tangent altitude. The calculations performed at Level-1 are specified not to include any correction for refraction, since it can only be adequately accounted for at Level-2. Hence geolocations assume no refraction, i.e. are as if no atmosphere is present.

3.6.4 Subsurface tangent points

The boresight tangent point will pass below the Earth surface as part of the proper operation of the instrument (in order that detector elements in the top part of the array can view the lowest part of the atmosphere). The returned geolocation will be in accord with the specification of PGS_CSC_GrazingRay (the mid point of the ray within the Earth), but this will be kept under review.

3.7 CELESTIAL BODIES IN FIELD OF VIEW

The moon and some bright planets and stars can enter both the atmospheric field of view of HIRDLS and also the field of view of the chopper reference port. (The orbital geometry of HIRDLS is such that contamination of the chopper reference by the moon will be a moderate frequency event.) It will be necessary to flag invalid all radiance measurements so affected. The SDP Toolkit routine PGS_CBP_body_inFOV provides an appropriate routine to determine which radiances are affected.

3.8 RADIOMETRIC CALIBRATION

The general approach to radiometric calibration has been discussed by C.W.P. Palmer in [SW- OXF-190B](#). This showed how the radiometric calibration relates to the overall instrument error budget. Measurements made in flight will be used to validate the mathematical model developed

in that paper. Here we are concerned only with the implementation of the algorithm derived from this mathematical model which will be used for in-flight calibration.

The radiometric calibration is based on measurements of two targets with known emission - space zero and the internal in-flight calibrator back body of known temperature (IFCBB_TMPn).

To correct for any non-linearity in the signal channel, the first step in processing will be to correct all the observed radiance channel counts (SIG_DAT_nn) as found necessary during pre-flight calibration. It is anticipated that this might involve at most a small quadratic correction but there should be no difficulty applying any well-determined correction at this stage of the processing. For each channel, nn=01,21, define the linearized counts

$$S = \text{linearize-function}_{nn} \{ \text{SIG_DAT_nn}, \text{SIG_ZERO_nn} \}$$

The calibrated radiance is then given simply by

$$\left(\frac{S - S_0(t)}{S_{BB}(t) - S_0(t)} \right) \left((1 - e_6)B(T_{BB})(t) + e_6B(T_{M6})(t) \right)$$

where

S is the observed radiance in linearized counts i.e. the linearized value of SIG_DAT_nn

e_6 is the emissivity of the calibrator mirror, M6. This will be measured during pre-flight calibration. The expected value is about 0.02.

B is the Planck function averaged over the spectral bandpass of the relevant channel. This function will be evaluated an extremely large number of times and would be computationally expensive to calculate formally. Either a table look-up or an approximation similar to that specified in Section 3.8.1 will be used.

$T_{BB}(t)$ is the effective temperature (K) of the in-flight calibrator black body. Three (platinum resistance thermometer) measurements of this temperature are available through conversion of the telemetry items IFCBB_TMP1, IFCBB_TMP2 and IFCBB_TMP3. These will be used in a method to be determined in pre-launch testing (possibly linear combination) to provide both a best estimate of the true value and a measure of its uncertainty.

$T_{M6}(t)$ is the temperature (K) of the calibrator mirror, M6. Two thermistors (telemetry items CALMIRTMP01 and CALMIRTMP02) and one platinum resistance thermometer (CALMIRTMP03) measure this quantity. It is expected that the CALMIRTMP03 value will be used for the calibration and the thermistors only for quality control.

$S_{BB}(t)$ is the linearized counts when observing the in-flight calibrator black body. The criteria (scan mirror position etc) to be used for selecting valid black body views will be determined before launch. This is derived using a Kalman filter from the linearized values of SIG_DAT_nn.

$S_0(t)$ is the linearized counts when observing space with the same scan mirror orientation used for measuring S. For each channel, the lowest tangent point altitude acceptable as a space view will be a constant input data parameter (e.g. 90km). This is derived by extrapolating the linearized values of SIG_DAT_nn as described below.

The emissivity of the in-flight calibrator black body has been assumed to be effectively unity (to be confirmed during pre-flight calibration).

Note that $T_{BB}(t)$, $T_{M6}(t)$, $S_{BB}(t)$, $S_0(t)$ have to be interpolated in time between the time of their measurement and the time of the observation S. The most appropriate way to do this

interpolation for the first three of these quantities is with a simple Kalman filter. This also generates an error estimate with each output value which can then be used in the computation of the radiance error discussed in [section 3.9](#).

$S_0(t)$ is treated somewhat differently. Many space view radiances are observed in each vertical scan. Figure 5 shows a typical radiance profile observed in a period of about 9 seconds. The altitude above which the radiance is effectively zero will be different for each channel but can be tabulated and provided as input calibration data.

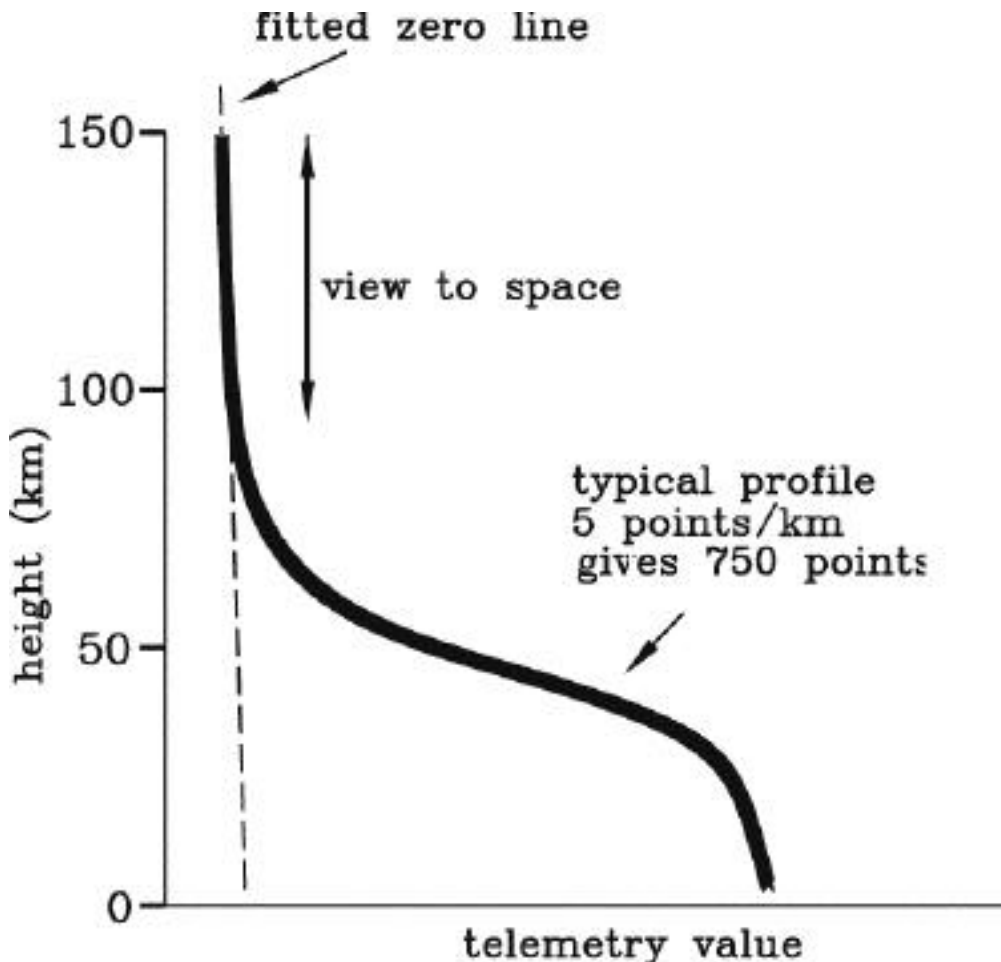


Figure 5.

Any systematic variation in the observed space view radiances will be extrapolated to the scan mirror position used for observation S. Initially this will be implemented using a linear regression of space view radiance with mirror elevation angle.

It is intended that the CHEM platform will be pitched down by at least 5 degrees so that all views through the "hot dog" aperture are "space views". By scanning in both azimuth and elevation, whilst viewing this constant radiometric target, a map of the variation in radiance with scan mirror position for each of the 21 channels can be built up. The azimuth of the in-flight calibrator black body is beyond the range of the hot-dog aperture so values in this region can only be obtained by extrapolation - a process which will need great care. It is expected that the pitch down manoeuvre will be repeated several times during the mission so that possible changes in the map can be observed. Such changes might be expected if the mirror surface became contaminated or otherwise degraded in any way. If the analysis of scan-dependent radiance data obtained during pitch down manoeuvres indicates that it is necessary, an alternative method of extrapolation may need to be devised.

3.8.1 APPROXIMATION to the INTEGRATION of the PLANCK FUNCTION

B(T), the Planck function for a given temperature, T, averaged over the spectral bandpass of the relevant channel has to be calculated many times during radiometric calibration. The following approximation was proposed by C.W.P. Palmer as an efficient way of calculating B(T). The Planck function, P(ν ,T), is a function of frequency, ν , and temperature, T.

Using units of nW/(cm².ster.cm⁻¹)

$$P(\nu,T) = c_1 \nu^3 / (\exp (c_2 \nu / T) - 1)$$

where $c_1=0.0011910439$ and $c_2=1.4387686$.

If the spectral bandpass function of each channel $F_n(\nu)$, is normalized so that the integral over all frequencies of $F_n(\nu) d\nu = 1$, then B is given by the integral over all frequencies of $F_n(\nu) P(\nu,T) d\nu$.

Defining the mean frequency of each channel, ν_{bar_n} , as the integral over all frequencies of $F_n(\nu) \nu d\nu$, we can evaluate B(T) using the approximation

$$B(T) = P(\nu_{bar_n},T) + 0.5 \frac{d^2P}{d\nu^2} d\nu^2$$

where $d\nu^2$ is the integral over all frequencies of $F_n(\nu) (\nu - \nu_{bar_n})^2 d\nu$.

Setting $c_3 = c_2 / T$,

$$\frac{d^2P}{d\nu^2} = P/\nu (3 + c_3 \exp (c_3 \nu) P / \nu^2)$$

so that B(T) can be evaluated as cubic polynomial of q.

$$q = \frac{P(\nu_{bar_n},T) / \nu_{bar_n}^2}{\exp (c_3 \nu_{bar_n}) - 1} = \frac{c_1 \nu_{bar_n}^3 / (\exp (c_3 \nu_{bar_n}) - 1)}{\nu_{bar_n}^2}$$

$$B(T) = c_1 q (\nu_{bar_n}^2 + 0.5 d\nu^2 (6 - c_5 q (6 + c_4 - 2c_5 q)))$$

where c_1 , $\nu_{bar_n}^2$ and $d\nu^2$ are constants defined above and

$c_4 = \exp (c_3 \nu_{bar_n})$ and $c_5 = c_3 c_4$ are both coefficients dependent on T.

The normalized spectral bandpass function of each channel $F_n(\nu)$ is the result of two separate filters: the warm filters at field stop #2 and the cold filters by the detectors. The temperatures of these filters are each recorded with three sensors (telemetry items LNS1WFTMP*, FPA_TMP_*) and $F_n(\nu)$ will be a function of both temperatures. The variation of the filter function with temperature will be measured during pre-launch testing and a parameterisation or tabulation will be provided for data processing activities.

3.9 ERROR ESTIMATION

The calibrated radiance is calculated using an expression of the form

$$R = (S - S_0) V / (S_B - S_0)$$

where V represents radiance from a "virtual" black body filling the hot-dog aperture. Treating S, S₀, S_B, V and their uncertainties as independent

$$\frac{dR}{dS} = V / (S_B - S_0)$$

$$\frac{dR}{dS_0} = (S - S_0) V / (S_B - S_0)^2 - V / (S_B - S_0) = (R - V) / (S_B - S_0)$$

$$\frac{dR}{dS_B} = -(S - S_0) V / (S_B - S_0)^2 = -R / (S_B - S_0)$$

$$\frac{dR}{dV} = (S - S_0) / (S_B - S_0) = R / V$$

So that the error variance of the calibrated radiance, sr^2 , is given by

$$sr^2 = (V^2 s^2 + (R - V)^2 s_0^2 + R^2 sb^2) / (S_B - S_0)^2 + R^2 sv^2 / V^2$$

where s^2 , s_0^2 , sb^2 and sv^2 are the error variances of S , S_0 , S_B and V respectively.

Detector noise, sd , is monitored by examination of the differences between signals from pairs of consecutive views of the same target. The time interval between these views (12ms) is so short that all instrument temperatures are effectively constant. Each difference provides a (poor) estimate of the variance but by meaning many such values the estimate is improved. sd will be estimated from k pairs of such measurements $S(t_{i-})$, $S(t_{i+})$, $i=1,k$ using

$$sd^2 = ((S(t_{1-}) - S(t_{1+}))^2 + (S(t_{2-}) - S(t_{2+}))^2 + \dots + (S(t_{k-}) - S(t_{k+}))^2) / 2k$$

In orbit, paired measurements can only be obtained from space views at a fixed mirror position or from views of the in-flight calibrator black body. It is likely that sd will vary slightly with S - so called signal-dependent noise. An effort will be made to characterise this in pre-launch testing and, if necessary, a method of parameterising $sd(S)$ from $sd(S_0)$ and $sd(S_B)$ will be implemented.

In the expression above for radiance error variance, sr^2 , s^2 will be given the appropriate value of sd^2 for a signal level S . Values of sb^2 are generated from the Kalman Filter used to interpolate measurements of S_B to the time of the observation S . The measurement error variance used in this Kalman Filter is the appropriate value of sd^2 .

Values of s_0^2 will be derived from the extrapolation of the space view to the scan mirror position used for observation S as described above.

sv^2 will be estimated from the In-Flight-Calibrator temperature telemetry.

4. PROCESSING CONSIDERATIONS

4.1 DATA VOLUMES

The volume of the Level 0 input data is about 648 Mbytes/day.

The calibration input data will be at most a few Mbytes and, in general, will not vary from day to day.

The Level 1 HIRDLS standard product output file is about 449 Mbytes/day.

The Level 1 Science Diagnostics file is estimated to be 264 Mbytes/day.

The Instrument Monitor File and the Calibration History file will be a few Mbytes/day.

4.2 NUMERICAL COMPUTATION CONSIDERATIONS

It is expected that the radiometric computation can be accomplished using standard 32-bit hardware arithmetic and standard intrinsic functions supplied by run-time libraries.

Geo-location calculations will require 64-bit precision as used in the SDP Toolkit routines. Calculations need to maintain precision equivalent to 1m at the tangent point. Although the

absolute location will be known less well than this, the relative locations are the major concern. The successive small rotations performed in section 3.5 may cause errors to accumulate, since a typical elevation profile will be 800 chopper revolutions long. It may be necessary to use quaternion representations and rotations.

If data are not available to adequate precision, it may be necessary to perform a local fit, e.g. of an arc. Given the spacecraft velocity of about 7000 m/s, relative temporal errors must be no more than tens of microsec so, again, a local fit may be necessary. This is not considered to be a significant problem provided that it is not overlooked and the requirements are understood.

The use of numerical algorithm or other libraries (other than the Toolkit) is not anticipated.

4.3 DATA FLOW

An overview of data flow is illustrated in Figure 6. Files are indicated by ellipses and processes by rectangular boxes. Arrows indicate the direction of data flow.

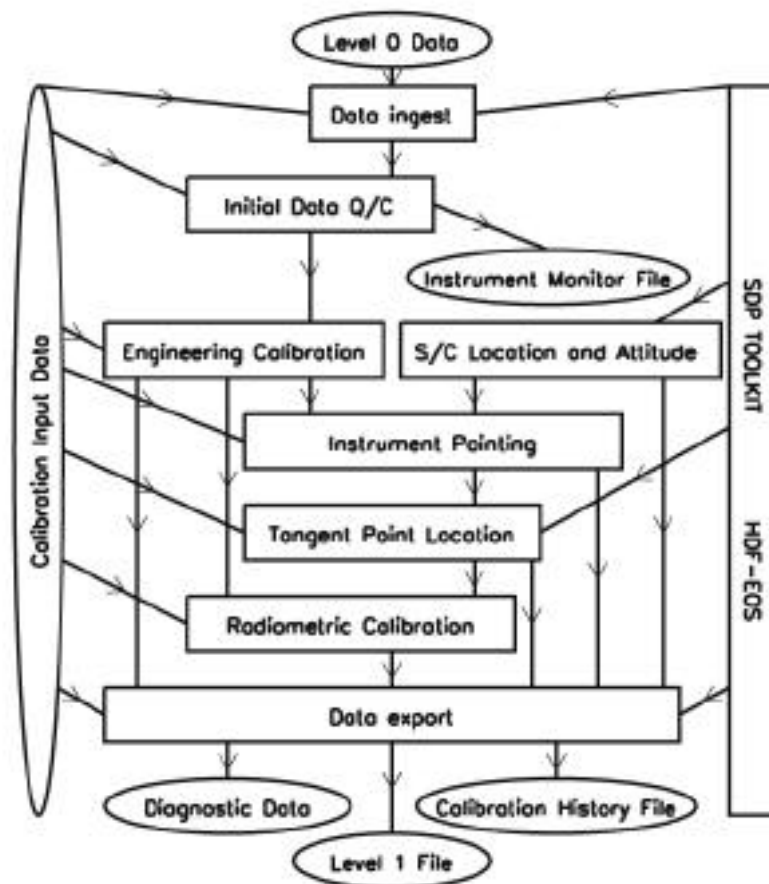


Figure 6.

4.4 FILE FORMATS

There is an ESDIS requirement that standard products should be stored in HDF-EOS structured files. HDF-EOS formats are special versions of the better-known Hierarchical Data Format (HDF). HIRDLS L1 files have been prototyped using HDF-EOS SWATH format following recommendations from the MOPITT team on EOS-AM.

Some diagnostic files which will be monitored and archived by the PI teams will be short ASCII files while others, which will be more voluminous and intended for machine-processing, HDF format files.

The retrieval process requires the location (latitude, longitude, altitude) of all 21 radiances in a chopper revolution together with other information such as solar zenith angle, geoid curvature and spacecraft location. To store all these values would require at least $(21 \times 7 + 3)$ variables, which, even using scaled int16 would require more than 2 Gbyte/day. The following approach attempts to reduce the storage requirement by assuming that routines from the SDP toolkit will be available to the L1-L2 processor and also analysis software to recalculate all the required location information with adequate precision. However, the source code of all routines involved in the L1-L2 processor should be portable to an environment where the full Toolkit (with such things as the spacecraft ephemeris) is not implemented. All data items not required for operational use at higher levels of processing will be written to a diagnostic file

L1 file contents

Data will be reported at four basic frequencies:-

HD: items required once per granule (assumed=calendar day)
MaF: items telemetered each major frame (64 chopper revolutions)
MiF: radiance error estimates each minor frame (8 chopper revolutions)
CR: items telemetered each chopper revolution

HDF Structure Name	Description	Variable Type	Bytes /MaF
CR data: (once per chopper revolution)			
Scaled Ch01 Radiance	Calibrated and scaled	SIG_DAT_01	int16 128
Scaled Ch02 Radiance	Calibrated and scaled	SIG_DAT_02	int16 128
Scaled Ch03 Radiance	Calibrated and scaled	SIG_DAT_03	int16 128
Scaled Ch04 Radiance	Calibrated and scaled	SIG_DAT_04	int16 128
Scaled Ch05 Radiance	Calibrated and scaled	SIG_DAT_05	int16 128
Scaled Ch06 Radiance	Calibrated and scaled	SIG_DAT_06	int16 128
Scaled Ch07 Radiance	Calibrated and scaled	SIG_DAT_07	int16 128
Scaled Ch08 Radiance	Calibrated and scaled	SIG_DAT_08	int16 128
Scaled Ch09 Radiance	Calibrated and scaled	SIG_DAT_09	int16 128
Scaled Ch10 Radiance	Calibrated and scaled	SIG_DAT_10	int16 128
Scaled Ch11 Radiance	Calibrated and scaled	SIG_DAT_11	int16 128
Scaled Ch12 Radiance	Calibrated and scaled	SIG_DAT_12	int16 128
Scaled Ch13 Radiance	Calibrated and scaled	SIG_DAT_13	int16 128
Scaled Ch14 Radiance	Calibrated and scaled	SIG_DAT_14	int16 128
Scaled Ch15 Radiance	Calibrated and scaled	SIG_DAT_15	int16 128
Scaled Ch16 Radiance	Calibrated and scaled	SIG_DAT_16	int16 128
Scaled Ch17 Radiance	Calibrated and scaled	SIG_DAT_17	int16 128
Scaled Ch18 Radiance	Calibrated and scaled	SIG_DAT_18	int16 128
Scaled Ch19 Radiance	Calibrated and scaled	SIG_DAT_19	int16 128
Scaled Ch20 Radiance	Calibrated and scaled	SIG_DAT_20	int16 128
Scaled Ch21 Radiance	Calibrated and scaled	SIG_DAT_21	int16 128

Elevation Angle	Boresight elevation SC frame (nanoradians)	int32	256
Azimuth Angle	Boresight azimuth SC frame(0.00005radians)	int16	128
Field Rotation	Detector array about boresight(0.00001deg)	int16	128
Gyro El Correction	Gyro correction to Elevation (nanoradians)	int16	128
Gyro Az Correction	Gyro correction to Azimuth(0.00005radians)	int16	128
Flags	Radiance and scan direction flags	int32	128
		Total bytes/MaF	3584

c. 403 Mbyte/day

MiF data: (once per minor frame, 8 chopper revolutions)

Scaled Ch01 Rad Error	Scaled error estimate for Ch01 radiance	int16	128
Scaled Ch02 Rad Error	Scaled error estimate for Ch02 radiance	int16	128
Scaled Ch03 Rad Error	Scaled error estimate for Ch03 radiance	int16	128
Scaled Ch04 Rad Error	Scaled error estimate for Ch04 radiance	int16	128
Scaled Ch05 Rad Error	Scaled error estimate for Ch05 radiance	int16	128
Scaled Ch06 Rad Error	Scaled error estimate for Ch06 radiance	int16	128
Scaled Ch07 Rad Error	Scaled error estimate for Ch07 radiance	int16	128
Scaled Ch08 Rad Error	Scaled error estimate for Ch08 radiance	int16	128
Scaled Ch09 Rad Error	Scaled error estimate for Ch09 radiance	int16	128
Scaled Ch10 Rad Error	Scaled error estimate for Ch10 radiance	int16	128
Scaled Ch11 Rad Error	Scaled error estimate for Ch11 radiance	int16	128
Scaled Ch12 Rad Error	Scaled error estimate for Ch12 radiance	int16	128
Scaled Ch13 Rad Error	Scaled error estimate for Ch13 radiance	int16	128
Scaled Ch14 Rad Error	Scaled error estimate for Ch14 radiance	int16	128
Scaled Ch15 Rad Error	Scaled error estimate for Ch15 radiance	int16	128
Scaled Ch16 Rad Error	Scaled error estimate for Ch16 radiance	int16	128
Scaled Ch17 Rad Error	Scaled error estimate for Ch17 radiance	int16	128
Scaled Ch18 Rad Error	Scaled error estimate for Ch18 radiance	int16	128
Scaled Ch19 Rad Error	Scaled error estimate for Ch19 radiance	int16	128
Scaled Ch20 Rad Error	Scaled error estimate for Ch20 radiance	int16	128
Scaled Ch21 Rad Error	Scaled error estimate for Ch21 radiance	int16	128
		Total bytes/MaF	336

c. 38 Mbyte/day

MaF data: (once per major frame, 64 chopper revolutions)

Time	Time of start of MaF	(TAI) float64	8
Latitude	Reference point latitude	(Degrees) float32	4
Longitude	Reference point long. ([-180,180]Degrees)	float32	4
Altitude	Reference point altitud e	(10metres) int16	2
View Direction	Boresight bearing at ref.pt.(0.01degrees)	int16	2
Solar Zenith Angle	Ref. pt. solar zenith angle (0.01degrees)	int16	2
Local Solar Time	Ref. pt. local solar time (0.001hours)	int16	2
Spacecraft Position	ECI coordinates at start of MaF	(cm) 3*int32	12
Spacecraft Velocity	ECI coordinates at start of MaF	(mm/s) 3*int32	12
Chopper Period		(microseconds) int16	2
Frame Counter	HIRDLS frame counter	int16	2
HIRDLS Clock		int16	2
Scan Mode Identifier	Scan mode identifier	int16	2
Warm Filter Temperature Calibrated	LNS1WFTMP*	(0.01K) int16	2
Cold Filter Temperature Calibrated	FPA_TEMP_*	(0.01K) int16	2
Wobble El Correction	Wobble cor. to elevation (nanoradians)	int16	2
Scan El Error	Elevation scan encoder error(nanoradians)	int16	2
Gyro El Error	Error in Gyro El Corrrrection(nanoradians)	int16	2
Wobble El Error	Error in Wobble El Correction(nanoradians)	int16	2
FIR Filter Index	Pointer to FIR filter coefficients	int16	2
		Total bytes/MaF	70

c. 7.9 Mbyte/day

HD data: (once per granule, day)

Data Date	Nominal data date	(TAI@00Z) float64	8
Ch01 Scale Factor	Scaling factor for Ch01 Rad and Rad_Error	float32	4
Ch02 Scale Factor	Scaling factor for Ch02 Rad and Rad_Error	float32	4
Ch03 Scale Factor	Scaling factor for Ch03 Rad and Rad_Error	float32	4
Ch04 Scale Factor	Scaling factor for Ch04 Rad and Rad_Error	float32	4

Ch05 Scale Factor	Scaling factor for Ch05 Rad and Rad_Error	float32	4
Ch06 Scale Factor	Scaling factor for Ch06 Rad and Rad_Error	float32	4
Ch07 Scale Factor	Scaling factor for Ch07 Rad and Rad_Error	float32	4
Ch08 Scale Factor	Scaling factor for Ch08 Rad and Rad_Error	float32	4
Ch09 Scale Factor	Scaling factor for Ch09 Rad and Rad_Error	float32	4
Ch10 Scale Factor	Scaling factor for Ch10 Rad and Rad_Error	float32	4
Ch11 Scale Factor	Scaling factor for Ch11 Rad and Rad_Error	float32	4
Ch12 Scale Factor	Scaling factor for Ch12 Rad and Rad_Error	float32	4
Ch13 Scale Factor	Scaling factor for Ch13 Rad and Rad_Error	float32	4
Ch14 Scale Factor	Scaling factor for Ch14 Rad and Rad_Error	float32	4
Ch15 Scale Factor	Scaling factor for Ch15 Rad and Rad_Error	float32	4
Ch16 Scale Factor	Scaling factor for Ch16 Rad and Rad_Error	float32	4
Ch17 Scale Factor	Scaling factor for Ch17 Rad and Rad_Error	float32	4
Ch18 Scale Factor	Scaling factor for Ch18 Rad and Rad_Error	float32	4
Ch19 Scale Factor	Scaling factor for Ch19 Rad and Rad_Error	float32	4
Ch20 Scale Factor	Scaling factor for Ch19 Rad and Rad_Error	float32	4
Ch21 Scale Factor	Scaling factor for Ch21 Rad and Rad_Error	float32	4
Nominal IFC Temperature	Nominal IFC temperature	(K) float32	4
Nominal CF Temperature	Nominal cold filter temperature	(K) float32	4
Nominal WF Temperature	Nominal warm filter temperature	(K) float32	4
Nominal Ch01 IFC Radiance		(W/m^2/sr) float32	4
Nominal Ch02 IFC Radiance		(W/m^2/sr) float32	4
Nominal Ch03 IFC Radiance		(W/m^2/sr) float32	4
Nominal Ch04 IFC Radiance		(W/m^2/sr) float32	4
Nominal Ch05 IFC Radiance		(W/m^2/sr) float32	4
Nominal Ch06 IFC Radiance		(W/m^2/sr) float32	4
Nominal Ch07 IFC Radiance		(W/m^2/sr) float32	4
Nominal Ch08 IFC Radiance		(W/m^2/sr) float32	4
Nominal Ch09 IFC Radiance		(W/m^2/sr) float32	4
Nominal Ch10 IFC Radiance		(W/m^2/sr) float32	4
Nominal Ch11 IFC Radiance		(W/m^2/sr) float32	4
Nominal Ch12 IFC Radiance		(W/m^2/sr) float32	4
Nominal Ch13 IFC Radiance		(W/m^2/sr) float32	4
Nominal Ch14 IFC Radiance		(W/m^2/sr) float32	4
Nominal Ch15 IFC Radiance		(W/m^2/sr) float32	4
Nominal Ch16 IFC Radiance		(W/m^2/sr) float32	4
Nominal Ch17 IFC Radiance		(W/m^2/sr) float32	4
Nominal Ch18 IFC Radiance		(W/m^2/sr) float32	4
Nominal Ch19 IFC Radiance		(W/m^2/sr) float32	4
Nominal Ch20 IFC Radiance		(W/m^2/sr) float32	4
Nominal Ch21 IFC Radiance		(W/m^2/sr) float32	4
TRCF to SFR Matrix	TRCF to SFR (3x3) Transformation Matrix	9*float64	72
FIR Coefficient Set 1	1st set of 32 FIR coefficients	32*float64	256
FIR Coefficient Set 2	2nd set of 32 FIR coefficients	32*float64	256
FIR Coefficient Set 3	3rd set of 32 FIR coefficients	32*float64	256
FIR Coefficient Set 4	4th set of 32 FIR coefficients	32*float64	256
FIR Coefficient Set 5	5th set of 32 FIR coefficients	32*float64	256
FIR Coefficient Set 6	6th set of 32 FIR coefficients	32*float64	256
FIR Coefficient Set 7	7th set of 32 FIR coefficients	32*float64	256
FIR Coefficient Set 8	8th set of 32 FIR coefficients	32*float64	256
			Total Bytes/granule 2308

Expected Size of L1 file = 449 Mbytes/day

Notes:-

'Radiance' and 'Rad Error' data items are expressed as fractions of the IFC radiance at a specified nominal temperature (TBD c290K). To exploit the dynamic range of int16 storage the following relationship is used

$$\text{Fractional IFC radiance} = (\text{Scaled radiance} + 16384) * \text{Scale Factor}$$

Scale factors are channel dependent but are typically about 0.00003.

The same scaling is used for 'Rad Error'.

Gyro and wobble corrections are included in the 'Elevation' and 'Azimuth' data but are also included as separate items in the L1 file so that these terms can be studied without re-running the L0-L1 processor.

'Field Rotation' is the angle between the detector array vertical and the plane defined by the bore-ray vector and a vector from the spacecraft to the earth centre (ECI origin). This is nominally zero.

Flags will indicate direction of vertical and horizontal scannings and flag bad radiance data.

Bit 0 - bit set if not part of nominal (10s) vertical scan
Bits 1-21 - bit set if corresponding rad_ value should not be used
 e.g. frame contains checksum/parity error etc
 radiance value contaminated (obstruction in FOV) etc
 radiance could not be calibrated
 detector elements too warm etc
Bits 22-25 - unused
Bit 26 - bit set if all channels contain valid space view
Bit 27 - bit set if valid IFC BB view
Bit 28 - bit set if scanning left (away from IFC)
Bit 29 - bit set if scanning right (towards IFC)
Bit 30 - bit set if scanning up (towards space)
Bit 31 - bit set if scanning down (towards earth)

The reference point is defined to be the boresight tangent point at the start of the major frame. All reference point data is nominal and is included only to allow easy data analysis and sub-setting where high accuracy is not required.

The nominal IFC radiance data are the radiances (in W/m²/sr) for each channel where the black body is at the nominal temperature ('Nominal IFC Temperature') and the filter functions are appropriate to the nominal filter temperatures ('Nominal WF Temperature' and 'Nominal CF Temperature'). This information is provided only so that the fractional radiances stored in the file can be quickly approximated in standard units.

One set of 32 FIR coefficients (the same for all channels) is used for each of four mission sub-modes: GM0 (21 channels sampled), SP1 (10 channels sampled), SP2 (7 channels sampled) and SP3 (3 channels sampled). The maximum number of sets of coefficients to be used in a day is TBD but a value of 8 has been used for prototyping activities.

Diagnostic file contents

Basically this contains all the calibrated data not in the L1 file.

Things that could be added include

- 1) Radiances calibrated without any non-linearity, or scan stray correction
- 2) Spacecraft ephemeris and attitude data

Things that might not be needed (but do not take much space) include

- 1) Telemetry from a few redundant systems
- 2) s/w build identifiers

There will be two data types:-

one for items telemetered each chopper revolution, CR

one for items telemetered each major frame, MaF, (64 chopper revolutions)

				Bytes
R data:				/MaF
clock_lsb		HIRCLKLSB	HIRDLS clock LSB	int*8 64
gyr_angle[0:3]	Calibrated	GYR*_ADAT	Gyro * angle data	4*int16 512
elev[1:2]	Calibrated	ELEVDATA	Elevation encoder *	2*int16 256
azim	Calibrated	AZIMDAT	Azimuth encoder	int16 128

				Bytes
MaF data:				
ifc_bb_temp[1:3]	Cal.	IFCBB_TMP*	IFC Black Body temp	3*int16 6
ifc_plate_temp	Calibrated	IFCBB_FRPL_TMP	IFCBB front plate temp	int16 2
ifc_oven_temp	Calibrated	IFC_OVEN_TMP	Ref. resistor oven temp	int16 2
ifc_p28_v	Calibrated	IFC_PSV_P28	IFC +28V rail volts	int16 2
ifc_p15_v	Calibrated	IFC_PSV_P15	IFC +15V rail volts	int16 2
ifc_n15_v	Calibrated	IFC_PSV_N15	IFC -15V rail volts	int16 2
ifc_p5_v	Calibrated	IFC_PSV_P5	IFC +5V rail volts	int16 2
sail_00_param[0:15]		SAILTASK00_*	SAIL Task 0 params	16*int16 32
sail_01_param[0:15]		SAILTASK01_*	SAIL Task 1 params	16*int16 32
sail_02_param[0:15]		SAILTASK02_*	SAIL Task 2 params	16*int16 32
sail_03_param[0:15]		SAILTASK03_*	SAIL Task 3 params	16*int16 32
sail_04_param[0:15]		SAILTASK04_*	SAIL Task 4 params	16*int16 32
sail_05_param[0:15]		SAILTASK05_*	SAIL Task 5 params	16*int16 32
sail_06_param[0:15]		SAILTASK06_*	SAIL Task 6 params	16*int16 32
sail_07_param[0:15]		SAILTASK07_*	SAIL Task 7 params	16*int16 32
sail_08_param[0:15]		SAILTASK08_*	SAIL Task 8 params	16*int16 32
sail_09_param[0:15]		SAILTASK09_*	SAIL Task 9 params	16*int16 32
sail_10_param[0:15]		SAILTASK10_*	SAIL Task 10 params	16*int16 32
sail_11_param[0:15]		SAILTASK11_*	SAIL Task 11 params	16*int16 32
sail_12_param[0:15]		SAILTASK12_*	SAIL Task 12 params	16*int16 32
sail_13_param[0:15]		SAILTASK13_*	SAIL Task 13 params	16*int16 32
sail_14_param[0:15]		SAILTASK14_*	SAIL Task 14 params	16*int16 32
sail_15_param[0:15]		SAILTASK15_*	SAIL Task 15 params	16*int16 32
sail_mem[504:511]		SAIL_SHM_*	SAIL shared memory	8*int32 32
sail_att_stat[0:3]		SAILCMDST_*	SAIL cmd att. status	4*int32 16
sail_pstatus		SAIL_PROC_STAT	SAIL Proc. Status	int8 1
sail_tstatus[0:15]		SAILTSKSTAT_*	SAIL Task Status	16*int8 16
sail_cmd_recd		SLCMDS_RCVCT	SAIL cmds: recvd count	int16 2
sail_cmd_reject		SLCMDS_REJCT	SAIL cmds: reject cnt.	int16 2
sail_cmd_result		SLCMD_LAST_RC	Last cmd: result code	int16 2
sail_cmd_number		SLCMD_LAST_CN	Last SAIL cmd: number	int16 2
gyr_temp[0:3]	Calibrated	GYR*_TEMP	Gyro temperatures	4*int16 8
gyr_board_temp[0:3]	Cal.	GYR*_BDTMP	Gyro board temps	4*int16 8
gyr_magnet[0:3]	Cal.	GYR*_MAGDAT	Magnetometer data	4*int16 8
gyr_capl[0:3]		GYR*_CAPL	Gyro cap loop output	4*int16 8
gyr_motor_v[0:3]	Cal.	GYR*_MOTV	Gyro motor volts	4*int16 8
gyr_motor_i[0:3]	Cal.	GYR*_MOTC	Gyro motor current	4*int16 8
gyr_status[0:3]		GYR*_STAT	Gyro status words	4*int16 8
gyr_p15_v[0:3]	Calibrated	GYR*_P15V	Gyro +15 volt levels	4*int16 8
gyr_n15_v[0:3]	Calibrated	GYR*_N15V	Gyro -15 volt levels	4*int16 8
sc_data[0:7]		ORB_DAT_*	S/C Ancillary data	8*int16 16
m1_temp[1:3]	Calibrated	M1TMP*	Pri. M1 mirror temp.	3*int16 6
chopper_temp[1:3]	Cal.	CHOPHSGTMP*	Chopper housing temp	3*int16 6
cal_mirror_temp[1:3]	Cal.	CALMIRTMP*	Cal. Mirror temps	3*int16 6
m2_temp[1:2]	Calibrated	M2TMP*	Sec. M2 mirror temp	2*int16 4
spv_mirror_temp[1:3]	Cal.	SPVUMIRTMP*	Chop. ref. Mir. temp	3*int16 6
struct_temp[1:4]	Cal.	STH_TMP_*	Structure temps.	4*int16 8
ccu_box_temp	Calibrated	CCUBOXTMP	CCU box temperature	int16 2
geu_box_temp	Calibrated	GEUBOXTMP	GEU box temperature	int16 2
pcu_box_temp	Calibrated	PCUBOXTMP	PCU box temperature	int16 2
beu_box_temp	Calibrated	BEUBOXTMP	BEU box temperature	int16 2
beu_mount_temp	Calibrated	BEUMNTTMP	BEU mount temperature	int16 2
spu_box_temp	Calibrated	SPUBOXTMP	SPU box temperature	int16 2
ipu_box_temp	Calibrated	IPUBOXTMP	IPU box temperature	int16 2
teu_box_temp	Calibrated	TEUBOXTMP	TEU box temperature	int16 2

teu_mount_temp	Calibrated	TEUMNTTMP	TEU mount temperature	int16	2
eea_mount_temp	Calibrated	EEAMNTTMP	EEA mount temperature	int16	2
eea_box_temp	Calibrated	EEABOXTMP	EEA box temperature	int16	2
sunsensor_temp[1:3]	Cal.	SUNSEN*_TMP	Sun sensor temps.	3*int16	2
door_angle	Calibrated	DOOR_POT	Door angle sensor	int16	2
door_safe	Calibrated	DOOR_SAF_ANG	Door Safe Angle setting	int16	2
wax_temp	Calibrated	SSHWA_TMP	Hot Wax Actuator temp.	int16	2
ssh_motor_temp	Calibrated	SSH_DORMOT_TMP	SSH drive motor temp.	int16	2
ssh_plate_temp	Calibrated	SSH_APL_TMP	SSH aperture plate temp	int16	2
ssh_pz_temp	Calibrated	SSH_PZSURF_TMP	SSH +Z surface temp.	int16	2
ssh_nz_temp	Calibrated	SSH_NZSURF_TMP	SSH -Z surface temp.	int16	2
ssh_status		SSH_STATUS	Sunshield switch status	int8	1
sva_status		SVA_STATUS	SVA switch status	int8	1
sva_motor_temp	Calibrated	SVA_DORMOT_TMP	SVA drive motor temp	int16	2
sva_plate_temp	Calibrated	SVA_MTGPLT_TMP	SVA mounting plate temp	int16	2
eea_status		EEA_STATUS	EEA config. status	int16	2
el_motor1_i[0:7]	Cal.	ELMOTR1_CRRT	Elev motor 1 current	8*int16	16
el_motor2_i[0:7]	Cal.	ELMOTR2_CRRT	Elev motor 2 current	8*int16	16
az_motor_i	Calibrated	AZMOTR_CRRT	Azimuth motor current	int16	2
chopper_i	Calibrated	CHOPMOT_CRRT	Chopper motor current	int16	2
teu_sw_status		TEU_TSW_STAT	Telescope S/W Status	int16	2
teu_proc_status		TEU_STATUS	TEU Processor Config.	int8	1
tss_hw_status		TSS_HW_CFG	TSS hardware config.	int16	2
tss_sigcon_status		TEU_SIGCON_STAT	TEU Sig Cond Data Acq	int8	1
scan_motor_status		SCAN_MOT_STAT	Scan Mir. motor status	int16	2
teu_adc_ref_v[0:3]	Cal.	TEU_ADC*_REF	TEU ADC +5V ref.	4*int16	8
teu_adc_zero_v[0:3]	Cal.	TEU_ADC*_ZER	TEU ADC +5V zero	4*int16	8
teu_p5_v	Cal.	TEU_P5V	TEU +5V rail voltage	int16	2
teu_p9_v	Cal.	TEU_P9V	TEU +9V rail voltage	int16	2
teu_n9_v	Cal.	TEU_N9V	TEU -9V rail voltage	int16	2
scan_mir_temp[1:3]	Cal.	SMTMP*	Scan mirror temps	3*int16	6
el_motor1_temp[1:2]	Cal.	ELMOT1TMP*	Elev. motor 1 temps	2*int16	4
el_motor2_temp[1:2]	Cal.	ELMOT2TMP*	Elev. motor 2 temps	2*int16	4
az_motor_temp	Cal.	AZMOTTMP	Azimuth motor temp	int16	2
oba_base_temp	Cal.	SCAN_BASE_TMP	OBA Scanner base temp	int16	2
oba_lens_temp[1:2]	Cal.	LNSASSY_TMP*	OBA lens asmbly temp.	2*int16	4
oba_baffle_temp	Cal.	SPVU_BAF_TMP	OBA Space View baffle	int16	2
oba_plate_temp	Calibrated	OBA_PLT_TMP	OBA aperture plate	int16	2
gmu_mount_temp	Calibrated	GMU_MNT_TMP	GMU Mount temperature	int16	2
gmu_house_temp	Calibrated	GMU_HSG_TMP	GMU Housing temp.	int16	2
tsw_build_id		TSW_CSCI_BUILD_	Telescope S/W Version	int16	2
fpa_temp[1:2]	Calibrated	FPA_TEMP_*	Focal Plane temps	2*int16	4
tmark_clock		TMARK_CLK	Time Mark clock word	int16	2
tmark_data		TMARK_DATA	Time mark data word	int16	2
sc_cmd_recd		SCCMDS_RCVCT	S/C cmds: received cnt.	int16	2
sc_cmd_reject		SCCMDS_REJCT	S/C cmds: reject count	int16	2
sc_cmd_result		SCCMD_LAST_RC	Last cmd: result code	int16	2
sc_cmd_number		SCCMD_LAST_CN	Last S/C cmd: number	int16	2
sc_cmd_packet		SCCMD_LAST_PC	Last packet. seq. cnt.	int16	2
macro_cmd_recd		MACMDS_RCVCT	Macro cmds: recd count	int16	2
macro_cmd_reject		MACMDS_REJCT	Macro cmds: reject cnt.	int16	2
macro_cmd_result		MACMD_LAST_RC	Last cmd: result code	int16	2
macro_cmd_number		MACMD_LAST_CN	Last Macro cmd: number	int16	2
minor_frame_count[0:7]		FRAMECNT	Minor frame count	8*int8	8
hsk_format[0:7]		HK_FORMAT_ID	H'keeping format	8*int16	16
sig_ser0[1:21]		SIG_ZERO_*	Signal chan offset	21*int16	42
spu_ap5_v[1:2]	Calibrated	SPU_P5VOLTS_*	SPU +5V (analog)	2*int16	4
spu_an5_v[1:2]	Calibrated	SPU_N5VOLTS_*	SPU -5V (analog)	2*int16	4
spu_dp5_v[1:2]	Calibrated	SPU_P5VOLTS_D*	SPU +5V (dig)	2*int16	4
spu_p12_v[1:2]	Calibrated	SPU_P12VOLTS_*	SPU +12V supply	2*int16	4
spu_n12_v[1:2]	Calibrated	SPU_N12VOLTS_*	SPU -12V supply	2*int16	4
ipu_p3_v	Calibrated	IPU_3P3VOLTS	Wkg IPU +3.3V supply	int16	2
ipu_p5_v	Calibrated	IPU_5VOLTS	Wkg IPU +5V supply	int16	2
ipu_p15_v	Calibrated	IPU_P15VOLTS	Wkg IPU +15V supply	int16	2

ipu_n15_v	Calibrated	IPU_N15VOLTS	Wkg IPU -15V supply	int16	2
ipu_p3_temp	Calibrated	IPU_3P3DDC_TMP	Wkg IPU +3.3V DDC temp	int16	2
ipu_p5_temp	Calibrated	IPU_5VDDC_TMP	Wkg IPU +5V DDC temp	int16	2
cmd_build_id		CMD_CSCI_BUILD_ID	Cmd S/W Buil ID	int16	2
tlm_build_id		TLM_CSCI_BUILD_ID	Telemetry S/W ID	int16	2
ipu_build_id		IPU_CSCI_BUILD_ID	IPU S/W ID	int16	2
sail_build_id		SAIL_CSCI_BUILD_ID	SAIL S/W ID	int16	2
css_op_status		CSS_OPSTATUS	Cooler operating stat.	int8	1
css_ddcag_status		CSS_DDCAG_STAT	Cooler DDC & cage stat.	int8	1
css_error_status		CSS_ERROR	Cooler error flags	int8	1
css_i	Calibrated	CSS_CURRENT	Cooler total current	int16	2
cryo_set	Calibrated	CRYOTIP_SETP	Cryo tip set point	int16	2
cryo_temp[0:1]	Calibrated	CRYOTIP_TMP_D0	Cryo tip temps	2*int16	2
css_freq_demand	Cal.	CSS_FREQ_DMD	Cooler freq. (demand)	int8	1
css_freq	Calibrated	CSS_FREQ_ACT	Cooler frequency	int16	2
css_phase_demand	Cal.	CSS_PH_DMD	Comp/Disp phase demand	int16	2
css_phase	Calibrated	CSS_PH_ACT	Comp/Disp phase	int16	2
comp_ampl_demand	Cal.	COMP_AMP_DMD	Comp amplitude(demand)	int16	2
comp_ampl	Calibrated	COMP_AMP_ACT	Comp amplitude(actual)	int16	2
disp_ampl_demand	Cal.	DISP_AMP_DMD	Disp amplitude(demand)	int16	2
disp_ampl	Calibrated	DISP_AMP_ACT	Disp amplitude(actual)	int16	2
radiator_temp[1:2]	Cal.	COOLRADTMP*	Cooler Rad. temps.	2*int16	2
compressor_temp	Cal.	COMPHEADTMP	Compressor head temp.	int16	2
displacer_temp[1:2]	Cal.	DISPL*TMP	Displacer temps.	2*int16	2
css_msg_number		CSS_MSG_NUMBER	CSS-IPS message number	int8	1
css_build_id		CSS_CSCI_BUILD_ID	Cooler F/W ID	int16	2
qbus_i[1:2]	Calibrated	QB*_CURRT	Quiet Bus currents	int16	2
spu_p5_v[1:2]	Calibrated	PSS_SPU_5V*	SPU +5V DDC* volts	2*int16	4
spu_p15_v[1:2]	Calibrated	PSS_SPU_P15V*	SPU +15V DDC* volts	2*int16	4
spu_n15_v[1:2]	Calibrated	PSS_SPU_N15V*	SPU -15V DDC* volts	2*int16	4
pcu_p5_v	Calibrated	PSS_PCU_5V	PCU Internal +5 Volts	int16	2
pcu_p15_v	Calibrated	PSS_PCU_P15V	PCU Internal +15V.	int16	2
pcu_n15_v	Calibrated	PSS_PCU_N15V	PCU Internal -15V.	int16	2
reg_p28_v[1:2]	Calibrated	PSS_REG_28V*	REG +28V DDC* volts	2*int16	4
sys_p5_v[1:2]	Calibrated	PSS_SYS_5V*	SYS +5V DDC A volts	2*int16	4
sys_p15_v[1:2]	Calibrated	PSS_SYS_15V*	SYS +15V DDC A	2*int16	4
sys_n15_v[1:2]	Calibrated	PSS_SYS_15V*	SYS -15V DDC A	2*int16	4
pss_status[0:7]		PSS_STATUS_*	PSS relay status	8*int16	16
spu_p5_temp[1:2]	Cal.	PSS_SPU_5V*TMP	SPU +5V* DDC temp	2*int16	4
spu_p15_temp[1:2]	Cal.	PSS_SPU_15V*TMP	SPU 15V* DDC temp	2*int16	4
reg_p28_temp[1:2]	Cal.	PSS_REG_28V*TMP	REG +28V* DDC temp	2*int16	4
sys_p5_temp[1:2]	Cal.	PSS_SYS_5V*TMP	SYS +5V* DDC temp	2*int16	4
sys_p15_temp[1:2]	Cal.	PSS_SYS_P15V*TMP	SYS +15V* DDC temp	2*int16	4
sys_n15_temp[1:2]	Cal.	PSS_SYS_N15V*TMP	SYS -15VA DDC temp	2*int16	4
pcu_p15_temp[1:2]	Cal.	PSS_PCU_15V*TMP	PCU 15V* DDC temp.	2*int16	4
qbus_filt_temp[1:2]	Cal.	PSS_Q*FILT_TMP	QBA Inrush Filt temp	2*int16	4
wobble_sensor[1:2]		WOBB_SENS*	Wobble sensor data	2*int16	4
wobble_box_temp	Cal.	WSEBOXTMP	WSE box temperature	int16	2

Total bytes/MaF 2086

c 235 Mbytes/day

4.5 QUALITY CONTROL AND DIAGNOSTICS

In-line quality control procedures, including telemetry item trending and limit checking, will be implemented as part of the Level 0-1 processor to provide an assessment of input data quality. In addition, this process will also provide supplementary information on long-term instrument performance to the HIRDLS team. Summary information collected during the processing of each Level 1 data granule will be reviewed by staff at the HIRDLS Science Computing Facility (SCF).

4.6 EXCEPTION HANDLING

The Level 0-1 processor must be robust enough to behave predictably when supplied with any corrupt data. Because of its origin and routing the raw L0 data can be a particular problem in this regard. Checksums and other data quality indicators will be inspected before any data are processed. Some further exception handling is effectively performed by the limit checking procedures mentioned in Section 4.5 above. Floating point exceptions should not be a major problem. Underflow to zero will be acceptable to all HIRDLS algorithms. Overflow is unlikely given the magnitude of the numbers in the telemetry will be limit checked. Code will be designed to avoid division by zero which is the most probable cause of a floating point exception in the Level 0-1 processor.

4.7 CODING STANDARDS

It is expected that the L0 to L1 processor will be written in Fortran because it is more familiar than C to those actively involved in this work. Similar coding standards will be applied to those used successfully with the ISAMS and MOPITT projects. Incremental features identified by the ANSI Fortran Language committee and recognised by ISO will not be used. To avoid unnecessary complexity and to assist in the task of long-term code maintenance use only of those constructs included in the ELF and F subset languages will be encouraged.

5. APPENDICES

5.1 APPLICABLE DOCUMENTS

The High Resolution Dynamics Limb Sounder (HIRDLS): an instrument for the study of global change. Gille, J. C. and J. J. Barnett, pp 439-450, in *The use of EOS for Studies for Atmospheric Physics*, ed Gille, J.C and G. Visconti, North Holland, Amsterdam, 1992.

[HIRDLS Instrument Technical Specification](#), SP-HIR-013T, January 1999.

HIRDLS Science Software Management Plan, SC-HIR-133, December 1997.

HIRDLS Science Data Management Plan, SC-HIR-135, December 1997.

[Theoretical Basis of the SDP Toolkit Geolocation Package for the ECS Project](#), 445-TP-002-002, May 1995, Hughes Information Technology Systems, Landover, Maryland.

[Version 2.0 SDP Toolkit Users Guide](#), 333-CD-100-001, June 1998, Raytheon Systems Company, Upper Marlboro, Maryland.

[HDF-EOS User's Guide for ECS Project Volume 1](#), 170-TP-100-001, June 1998, Hughes Information Technology Systems, Landover, Maryland.

[HDF-EOS User's Guide for ECS Project Volume 2](#), 170-TP-101-001, June 1998, Hughes Information Technology Systems, Landover, Maryland.

5.2 CHEM-1/SOLSTICE ATBD REVIEW, MAY 18-19, 1999.

5.2.1 Questions Received Prior to Oral Presentation

12 May 1999

1. The value of the gyro is questioned. The system still seems to be limited by mirror encoder error. The gyro can only help with movements that will perfectly couple to the mirror (at a frequency less than chopper rotation). However, it is not likely to be critical to results. Twenty-metre precision on pressure surfaces over 500km seems unlikely.
2. Channel alignment - How will attitude be verified in orbit, especially considering the curved limb ?
3. No FOV functions are shown. What will be their shape and how will they be calibrated ?
4. Signal offset variation as a function of view direction could contain thermal dependencies. How will this be addressed ?
5. How will off-axis scatter be monitored, and calibrated in orbit if necessary ?
6. How will filter bandpass temperature dependence be handled ?
7. No discussion of instrument time response is presented. We assume the bandpass will be very wide, but if wider than the sampling nyquist, S/N will be sacrificed.

5.2.2 Outline of responses given at Oral Presentation

18 May 1999

1. The use of gyroscopes is fundamental to the instrument design. However accurate the mirror encoder this only measures position relative to the optical bench and, on a spacecraft such as CHEM which will be subject to a lot of vibration, it is essential that the motion of the optical bench is measured as well as possible. Gyroscopes provide a suitable method of doing this.

The scan mirror elevation encode will be much more precise than the question suggested, with a single sample r.m.s. errors of approximately 0.4 arcsec line-of-sight, which corresponds to 6m at the tangent point. Without gyro measurements, the motions of the optical bench would be the dominant source of pointing error.
2. Channel alignment may be verified in orbit by observation of bright celestial bodies. During the discussion it was suggested that the Earth surface could sometimes be used over deserts and possibly the Antarctic plateau; ISAMS was believed to have seen the surface over deserts.
3. The instrument field of view is not used in the Level 0 - 1 processing and consequently is not addressed in this ATBD. The field of view of each channel will be measured in pre-launch testing. Two possible methods by which this information may be used in the forward model in Level 1 - 2 processing have been identified (ref. ATBD-HIRS-02).
4. [Section 3.8](#) Radiometric Calibration does not make it clear that an estimate of the variation of signal offset with view direction is made each vertical scan (roughly every 10 seconds). The thermal characteristics of the (thermostated) instrument are expected to vary primarily at orbital rate (roughly every 6000 seconds). It is expected that this information will enable us to model any thermal dependencies. The approach to the

correction for scan-dependent radiances will be validated during spacecraft "pitch down" manoeuvres.

5. The effect of scatter inside of the scan mirror should be completely corrected for by in-orbit calibration when the view is to space (assumed zero radiance) obtains the zero radiance signal. This is because the viewing geometry remains constant.

Outside the scan mirror, the viewing geometry remains relatively constant within each elevation scan, hence to a good approximation the effect of scatter will also be taken out by using the space view signal for the given azimuth angle as a zero point calibration for that same azimuth angle. This will be measured as part of the scanning sequence for measuring the profile; hence every profile will have its own near-coincident set of zero radiance signal measurements. However it is accepted that there will be factors (notably scatter from the scan mirror and variation of scan mirror emissivity with mirror angle) which cause a variation of the zero radiance signal with mirror angle. Hence provision is being made for making a correction: the scan mirror will be moved sufficiently far (20km TBV) above the lowest tangent altitude needed to obtain an effective zero radiance view so that the rate of change of signal with elevation angle can also be obtained as described in [Section 3.8](#). This trend can then be applied to lower altitudes. It will be possible to enable or disable this feature in data processing. Study of the variation of space signal zero thus obtained with azimuth and possibly latitude and longitude should enable information about scattering and mirror emissivity to be obtained by offline processing, including by fitting against models which incorporate the expected variations.

6. See last paragraph of [Section 3.8](#) Radiometric Calibration. Note that the band-defining warm filter is thermostatted.
7. The signal processing chain involves an analogue system including analogue filters which produce a digitised data value every half chopper cycle (at a phase relationship which is commandable separately for each channel), i.e. 1000 samples per second. These data are filtered in the instrument processor using a FIR filter with coefficients which can be changed by command, to lead to a telemetered data value every chopper rotation, i.e. 6 chopper cycles or 12msec nominal. The FIR filter coefficients will be selected with a trade-off study jointly to maximise the vertical resolution and minimise noise, and this is expected to have the effect that each radiometric sample is nearly independent of its neighbour.

5.2.3 Recommendations received from the Review Panel

15 July 1999

The HIRDLS Executive Summary of the EOS CHEM-1 [ATBD Review Panel Report](#) did not distinguish between the two ATBDs presented. Of the total of seven recommendations only three might be applied to HIRS-ATBD-01.

"Embarking on a new development could delay the start of detailed modeling of retrieval errors in a full-up system. The required fidelity and accuracy performance may take years to achieve, considering the likely limited time available to those on the team who are capable of developing such models."

- "Recommendation 1 - Evaluate available code before embarking on new development. Even if performance is marginal, put code in place to allow rapid and robust processing simulations to commence ASAP. Insert new developments as they become available."

"The mission is depending on gyro information and real-time spacecraft attitude information for reliable channel alignment, which is crucial to accurate retrievals"

- "Recommendation 3 - Position identical CO₂ bandpass filters on opposite sides of the detector focal plane (duplicate CO₂ channels) and offset in the vertical. This allows alignment of these CO₂ channels to be inferred from the data, effectively validating the channel alignment process. They also serve as a backup method of channel alignment should gyro and attitude data become unreliable. By offsetting in the vertical, they could serve as sensors for attitude motion in the scan plane, although care must be taken to distinguish motion from twist about the boresight and Earth oblateness effects."

"There are two important aspects of the HIRDLS instrument which have direct impact on the successful operation of the instrument. One is the ability to use a model of scan mirror response versus scan angle to extrapolate the calibration information provide [sic] by viewing the IFC to limb scenes. The HIRDLS plan is to determine the mirror response using orbital maneuvers to make azimuthal and elevation scans of deep space. These measurements would then be input to a response versus scan angle model of the scan mirror, the output of which would be applied in the calibration of various limb data. Preflight, laboratory measurements of the reflectance (or emissivity) of the the scan mirror at the azimuthal/elevation angles corresponding to views of the IFC could be compared to lab measurements at limb viewing angles. However, extrapolation of these preflight measurements to the on-orbit situation requires some assumptions concerning the presence or lack of on-orbit directional degradation of mirror reflectance. The HIRDLS instrument and science team are well aware of these challenges."

"The second important aspect of the HIRDLS instrument is the potential launch/on-orbit registration-related problem of the focal plane shifting relative to the instrument optics. During the discussion of this topic, views of the Moon, stars, and strategically selected portions of Antarctica were suggested as means to provide registration information in the event of a focal plane/optics shift. This strategy needs to be examined more closely and developed more fully."

- "Recommendation 5 - Look at ways to verify that internal offset is constant with scan mirror position. It appears that this is assumed for the IFC look position. Estimate possible error due to this assumption."

5.2.4 Responses to Review Panel Recommendations

Recommendation 1:

No significant code has been identified which could be re-used for HIRDLS Level 0 - Level 1 processing. Obviously experience and ideas developed for ISAMS and for the HIRDLS calibration and test facility will be exploited wherever appropriate.

Recommendation 3 - from John Barnett, HIRDLS UK PI :-

The point is taken; however the time when such changes could have been made in the focal plane design passed at least a year ago because of the long lead time on the manufacture. To have added elements to the set of 21 would have caused optical problems, hence there would have been a very difficult decision as to which of the current passbands to replace. Currently it is believed that the pointing knowledge obtained from the gyroscope subsystem will be sufficient, after special in-orbit calibrations to determine small constant offsets. It should be noted that the 5 temperature sounding channels in the 15 micron carbon dioxide band were all placed in the same (central) column of the array specifically to provide sets of radiances which are mutually self consistent to a very high degree, i.e. for the sort of considerations mentioned by the Panel.

Recommendation 5 - from Christopher W P Palmer, HIRDLS Instrument Calibration Scientist :-

The Panel have correctly identified two concerns of the HIRDLS instrument and science team in the area of radiometric calibration and forward modelling. However the concern as stated is incorrect in detail.

1. Effects due to variation of Scan Mirror properties with angle.

There is an issue here, but it does not relate to gain calibration as such. The variation of reflectance with angle of incidence is extremely small for a good reflector: for a clean metal surface with normal reflectance of 97.0%, the (polarization averaged) reflectance at 40 degrees is 96.9%, a variation which is probably less than the precision of pre-launch reflectance data. The upper limit in gain error from this source is thus 0.1%, and this is in fact a considerable overestimate because of a fundamental radiometric compensation mechanism - the gain error consists of this reflectance change multiplied by the fractional difference in Planck function between scan mirror and IFC, which reduces the error by about a factor of 5. This makes it a very small component of the overall gain error budget (1% total), and questions of extrapolating mirror properties to the IFC view are simply irrelevant.

The concern relates to the consequent angle-variation in emission by the scan mirror, which leads to a variable offset. This error is only significant for scenes with low radiance (high altitude or aerosol channels). The offset variation is, in the worst cases, a few times the random noise, and will be handled as described in section 3.8. Data from orbital manoeuvres may be used to validate this procedure.

2. Possible launch shift of focal plane/optics alignment.

This is recognised as a critical area, as microns of relative movement between the focal plane assembly and the remainder of the optics can lead to changes in either overall line-of-sight or defocus. In fact the more significant error may well be the defocus. Overall absolute alignment knowledge is not required to high accuracy, only relative alignment changes between views, and between channels. Launch shifts in channel co-alignment are unlikely, and post-launch changes on the overall alignment of the (thermostatted) focal plane are not expected. However some change in the as-measured field-of-view shapes due to launch shifts is possible, and the treatment of field-of-view in Level 2 must take account of this. Special observations of the Moon or selected surface targets are unlikely to give useful data on absolute alignment (unless the change is so gross that we have no idea where we are looking) as the instrument is a radiometer and not an imager, and are even less likely to give useful data on FOV shape, as the measurement conditions are inadequately controlled.

In addition, we share many of the general concerns expressed in the report (Section II.3). In particular we note the comments about systematic errors and agree that more emphasis needs to be placed on the reduction of these. However, the treatment of systematic errors often entails off-line analysis of flight data and does not form part of the data processing algorithms described in the ATBD.

5.3 ACRONYMS and ABBREVIATIONS

CSS	Cooler Sub-System
ECI	Earth Centered Inertial Reference Frame (J2000)

ECIS ECI reference frame with instantaneous with spacecraft velocity
FPA Focal Plane Assembly
GEU Gyroscope Electronics Unit
GMU Gyroscope Mounting Unit
HIRDLS High Resolution Dynamics Limb Sounder (EOS CHEM experiment)
IFC In-Flight Calibrator
IFOV Instrument Field Of View
IPU Instrument Processor Unit
IRCF Instrument Reference Coordinate frame
ISAMS Improved Stratospheric and Mesospheric Sounder (UARS experiment)
ISO International Standards Organisation
LIMS Limb Infrared Monitor of the Stratosphere (NIMBUS 7 experiment)
MOPITT Measurement of Pollution in The Troposphere (EOS AM experiment)
OBA Optical Bench Assembly
POA Principal Optical Axis
PSS Power Sub-System
SAIL Science Algorithm Implementation Language
SCF Science Computing Facility
SDP Science Data Processing
SFR Spacecraft Frame of Reference
SPU Signal Processing Unit
SRCF Spacecraft Reference Coordinate Frame
SSH Sun-Shield
SVA Space View Aperture
TEU Telescope Electronics Unit
TRCF Telescope Reference Coordinate Frame
TSS Telescope Sub-System
UARS Upper Atmosphere Research Satellite